Cosmological constraints on Λ_sCDM scenario in a type II minimally modified gravity

Özgür Akarsu[1,*] Antonio De Felice[2,†] Eleonora Di Valentino[3,‡] Suresh Kumar[4,§] Rafael C. Nunes[5,6,‖]
Emre Özülker,[1,3,¶] J. Alberto Vazquez[7,**] and Anita Yadav[8,††]

[1]*Department of Physics, Istanbul Technical University, Maslak 34469 Istanbul, Türkiye*
[2]*Center for Gravitational Physics and Quantum Information, Yukawa Institute for Theoretical Physics,*
Kyoto University, 606-8502, Kyoto, Japan
[3]*School of Mathematics and Statistics, University of Sheffield,*
Hounsfield Road, Sheffield S3 7RH, United Kingdom
[4]*Data Science Institute, Plaksha University, Mohali, Punjab-140306, India*
[5]*Instituto de Física, Universidade Federal do Rio Grande do Sul,*
91501-970 Porto, Alegre Rio Grande do Sul, Brazil
[6]*Divisão de Astrofísica, Instituto Nacional de Pesquisas Espaciais,*
Avenida dos Astronautas 1758, São José dos Campos, 12227-010, São Paulo, Brazil
[7]*Instituto de Ciencias Físicas, Universidad Nacional Autónoma de México,*
Cuernavaca, Morelos, 62210, México
[8]*Department of Mathematics, Indira Gandhi University, Meerpur, Haryana 122502, India*

The idea of a rapid sign-switching cosmological constant (mirror AdS-dS transition) in the late universe at $z \sim 1.7$, known as the Λ_sCDM model, has significantly improved the fit to observational data and provides a promising scenario for alleviating major cosmological tensions, such as the H_0 and S_8 tensions. However, in the absence of a fully predictive model, implementing this fit required conjecturing that the dynamics of the linear perturbations are governed by general relativity. Recent work embedding the Λ_sCDM model with the Lagrangian of a type II minimally modified gravity known as VCDM has propelled Λ_sCDM to a fully predictive model, removing the uncertainty related to the aforementioned assumption; we call this new model Λ_sVCDM. In this work, we demonstrate that not only does Λ_sCDM fit the data better than the standard ΛCDM model, but the new model, Λ_sVCDM, performs even better in alleviating cosmological tensions while also providing a better fit to the data, including cosmic microwave background, baryon acoustic oscillations, type Ia supernovae, and cosmic shear measurements. Our findings highlight the Λ_sCDM framework, particularly the Λ_sVCDM model, as a compelling alternative to the standard ΛCDM model, especially by successfully alleviating the H_0 tension. Additionally, these models predict higher values for σ_8, indicating enhanced structuring, albeit with lower present-day matter density parameter values and consequently reduced S_8 values, alleviating the S_8 tension as well. This demonstrates that the data are well fit by a combination of background and linear perturbations, both having dynamics differing from those of ΛCDM. This paves the way for further exploration of new ways for embedding the sign-switching cosmological constant into other models.

I. INTRODUCTION

The standard ΛCDM model has been remarkably consistent with the majority of data from astrophysical and cosmological observations conducted over the past decades [1–7]. However, in the new era of high-precision cosmology, certain discrepancies, such as the H_0 tension [8,9] reaching to 5σ level of significance [10–12] and the S_8 tension reaching 3σ [4,13–20], along with some others of lesser significance, have emerged when analyzing different datasets, bringing the standard model to a crossroads. This pivotal situation has compelled the scientific community to

[*]Contact author: akarsuo@itu.edu.tr
[†]Contact author: antonio.defelice@yukawa.kyoto-u.ac.jp
[‡]Contact author: e.divalentino@sheffield.ac.uk
[§]Contact author: suresh.kumar@plaksha.edu.in
[‖]Contact author: rafadcnunes@gmail.com
[¶]Contact author: ozulker17@itu.edu.tr
[**]Contact author: javazquez@icf.unam.mx
[††]Contact author: anita.math.rs@igu.ac.in

embark on a quest for alternative explanations, either rooted in novel physics or through the identification of potential systematic errors in the data. For recent reviews, see Refs. [21–28].

Along the path of seeking novel physics as an explanation for cosmological tensions, many attempts have been made; see, e.g., Refs. [21–23] and references therein for a comprehensive but not exhaustive list. Most of these rely on a bottom-up approach, assuming the existence of some effective field theory that could account for the phenomenology assumed. In this approach, distinguishing between the many possible models can be achieved by identifying which model best fits the observational data. In this sense, one of the most promising ideas is the recently proposed Λ_sCDM theory-framework, which considers the possibility that the Universe has recently (at redshift $z \sim 2$) undergone a rapid *mirror* anti–de Sitter (AdS) vacuum to a de Sitter (dS) vacuum transition (a sign-switching of the cosmological constant, Λ_s) [29–33]. This simple paradigm, standing as one of the most economical approaches (introducing only one additional parameter on top of ΛCDM, $z_\dagger$, the redshift of the AdS-dS transition) for the simultaneous resolution of major cosmological tensions in the literature so far, can indeed account for a plethora of different datasets, as we will also see in this work, and it attracts interest from both theoretical and observational points of view. The suggested rapid nature of the sign-switching cosmological constant, along with its shift from negative to positive values, has generally found challenging in identifying a concrete physical mechanism. However, the phenomenological success of Λ_sCDM, despite its simplicity, has led to increasing interest in introducing theoretical approaches for the realization of the late-time mirror AdS-dS(-like) transition. It was shown in [34–36] that although the AdS swampland conjecture suggests that AdS-dS transition in the late universe seems unlikely (due to the arbitrarily large distance between AdS and dS vacua in moduli space), it can be realized through the Casimir forces of fields inhabiting the bulk. Furthermore, it was demonstrated in [37] that in various formulations of GR, it is possible to obtain a sign-switching cosmological constant through an overall sign change of the metric. Recently, in [38], the authors proposed embedding the late time mirror AdS-dS transition into the theoretical framework of VCDM [39–44], a minimal theory of gravity, i.e., a model that does not introduce extra degrees of freedom into the theory. The result of this embedding leads to a theory that we will call the Λ_sVCDM model. In this way, Λ_sCDM has become a fully predictive model with the ability to describe all gravitational phenomena, including the cosmological evolution of our Universe. We refer readers to Refs. [45–65] for more works that study dark energy assuming negative density values, (mostly) consistent with a negative (AdS-like) cosmological constant, for $z \gtrsim 1.5$–2, particularly aiming to address cosmological tensions such

as the H_0 and S_8 tensions and, recently, anomalies from JWST, and to Refs. [66–84] suggesting such dynamics for dark energy from model-independent/nonparametric observational reconstructions and investigations.

In this paper, we will explore how implementing Λ_sCDM into a model affects cosmological observables, particularly concerning the H_0 [8,10,11,21] and S_8 [13,20] tensions. The Λ_sCDM model, considered within the framework of general relativity, alters the background dynamics compared to ΛCDM without modifying the equations of motion for the perturbations. In contrast, the Λ_sVCDM model has a well-defined Lagrangian, which generally leads to differences from ΛCDM in both the background and perturbation equations of motion. Specifically, Λ_sVCDM is defined as the model introduced in [38], sharing the same background as Λ_sCDM but with one additional parameter compared to ΛCDM: the redshift at which the transition occurs.

Since the observables we consider depend on both the background and cosmological linear perturbation dynamics, it is expected that Λ_sCDM and Λ_sVCDM will, in general, yield different constraints from the data. Even if Λ_sCDM provides a good fit to the data (compared to ΛCDM), it is not clear *a priori* whether a full model implementation of Λ_sCDM, namely Λ_sVCDM, will continue to provide a good fit to the data. Therefore, to address this uncertainty, we will compare ΛCDM, Λ_sCDM, and Λ_sVCDM using the same datasets in this paper.

The paper is organized as follows. In Sec. II, we present the scenarios explored in this work, namely the Λ_sCDM and Λ_sVCDM. In Sec. III, we outline the datasets and the methodology used to analyze these scenarios. In Sec. IV, we discuss the results obtained. Finally, in Sec. V, we derive our conclusions.

II. Λ_sCDM PARADIGM AND ITS IMPLEMENTATION INTO THE VCDM MODEL

The Λ_sCDM paradigm is inspired by the recent conjecture that the universe underwent a spontaneous mirror AdS-dS transition characterized by a sign-switching cosmological constant (Λ_s) around $z \sim 2$ [29–33]. This conjecture emerged following findings in the *graduated dark energy* (gDE) model [29], which demonstrated that a rapid smooth transition from an AdS-like dark energy to a dS-like dark energy at $z \sim 2$ could address the H_0 and BAO Ly-α discrepancies [29]. It involves replacing the usual cosmological constant (Λ) of the standard ΛCDM model with a sign-switching cosmological constant, which can typically be described by sigmoid functions, such as the well-known smooth approximation of the signum function, $\text{sgn } x \approx \tanh kx$, for a constant $k > 1$, where x can represent either redshift (z) or scale factor ($a = 1/(1 + z)$, assuming Robertson-Walker metric). For instance, $\Lambda_s(z) = \Lambda_{\text{dS}} \tanh[\eta(z_\dagger - z)]$, where $\eta > 1$ determines the rapidity of the transition, and $\Lambda_{\text{dS}} = \Lambda_{s0}/\tanh[\eta z_\dagger]$. For a fast transition (e.g., for $\eta \gtrsim 10$) around

$z_\dagger \sim 1.8$, one can safely take $\Lambda_{dS} \approx \Lambda_{s0}$. In the limit as $\eta \to \infty$, we approach the *abrupt* Λ_sCDM model, which has been commonly investigated in the literature [30–32], presenting a one parameter extension of the standard ΛCDM model; namely,

$$\text{(abrupt) } \Lambda_s\text{CDM}: \Lambda_s(z) \to \Lambda_{s0}\, \text{sgn}[z_\dagger - z] \quad \text{for } \eta \to \infty \tag{1}$$

where $\Lambda_{s0} > 0$ is the present-day value of $\Lambda_s(z)$, serving as an idealized depiction of a rapid mirror AdS-dS transition. Originally, this limit case of the model was considered phenomenologically within the framework of general relativity (GR) in [30–32]. However, without a model, i.e., without an explicit Lagrangian, the paradigm could not be checked against other observables, such as solar system constraints or cosmological linear perturbation theory. Recently, the Λ_sCDM idea was realized within a type II minimally modified gravity model, VCDM. Henceforth, we refer to the original idea based on GR (that is, conjecturing no change in the dynamics of the linear perturbation equations) as Λ_sCDM, and the new realization within the model of VCDM as Λ_sVCDM [38]. In this paper, we consider a smooth (implied by finite η) Λ_sVCDM model that exhibits a *quiescent mirror AdS-dS transition*, to be compared with the standard ΛCDM and abrupt Λ_sCDM (1) models, using the following functional for $\Lambda_s(a)$

$$\Lambda_s\text{VCDM}: \Lambda_s(a) = \Lambda_{dS} \tanh[\zeta(a/a_\dagger - 1)], \tag{2}$$

where we fix $\zeta = 10^{1.5}$ to study a fast transition that mimics the background of the abrupt Λ_sCDM model as closely as possible while maintaining the same number of free parameters as the abrupt Λ_sCDM, with only one additional parameter, $z_\dagger$, determining the AdS-dS transition redshift, compared to the standard ΛCDM.[1,2] The primary distinction between the Λ_sCDM and Λ_sVCDM models considered here is that Λ_sVCDM is explicitly derived from a well-defined Lagrangian, which uniquely characterizes the model, whereas Λ_sCDM does not possess a Lagrangian formulation. For a detailed theoretical construction of the Λ_sVCDM model, we refer readers to Ref. [38], and for the VCDM theory in which it is embedded, to Refs. [39,40], while a concise overview is provided in the Appendix for convenience.

---

[1]Larger finite values of ζ are in principle possible but would not be distinguishable with the cosmological data currently available.

[2]Note that, for $\zeta = \eta(1 + z)$, Eq. (2) is equivalent to $\Lambda_s(z) = \Lambda_{dS} \tanh[\eta(z_\dagger - z)]$, but since both η and ζ are parameters that are relevant around $z \sim z_\dagger$ for a very rapid transition as assumed here, this seemingly dynamic transformation is effectively a simple scaling, $\zeta \approx \eta(1 + z_\dagger)$.

III. DATASETS AND METHODOLOGY

To constrain the model parameters, we performed Markov Chain Monte Carlo (MCMC) analyses using a modified version of the publicly available CLASS+MontePython code [85–87]. We employed the $R - 1 < 0.01$ Gelman-Rubin criterion [88] to ensure the convergence of our MCMC chains. We analyzed the samples using the GetDist Python module.

Our parameter space consists of six parameters common with the standard ΛCDM model, namely, the present-day physical density parameters of baryons $\omega_b \doteq \Omega_b h^2$ and cold dark matter (CDM) $\omega_{cdm} \doteq \Omega_{cdm} h^2$, the angular size of the sound horizon at recombination θ_s, the amplitude of the primordial scalar perturbation $\log(10^{10} A_s)$, the scalar spectral index n_s, and the optical depth τ_{reio}. Additionally, we consider the redshift $z_\dagger$ at which the sign-switching Λ_s occurs. We use flat priors for all parameters in our statistical analyses: $\omega_b \in [0.018, 0.024]$, $\omega_{cdm} \in [0.10, 0.14]$, $100\theta_s \in [1.03, 1.05]$, $\ln(10^{10}A_s) \in [3.0, 3.18]$, $n_s \in [0.9, 1.1]$, $\tau_{reio} \in [0.04, 0.125]$, and $z_\dagger \in [1, 3]$.

The datasets used are as follows:

(i) CMB: The CMB dataset from the Planck 2018 legacy release is a comprehensive dataset, widely recognized for its precision and accuracy. We use CMB temperature anisotropy and polarization power spectra measurements, their cross-spectra, and lensing power spectrum [89,90], namely, the high-ℓ Plik likelihood for TT ($30 \leq \ell \leq 2508$) as well as TE and EE ($30 \leq \ell \leq 1996$), the low-ℓ TT-only likelihood ($2 \leq \ell \leq 29$) based on the Commander component-separation algorithm in pixel space, the low-ℓ EE-only likelihood ($2 \leq \ell \leq 29$) using the SimAll method, and measurements of the CMB lensing. We refer to this dataset as Planck.

(ii) BAO: We utilize the baryon acoustic oscillation (BAO) measurements reported in Table I, which consists of both isotropic and anisotropic BAO measurements. The isotropic BAO measurements are identified as $D_V(z)/r_d$, where $D_V(z)$ characterizes the spherically averaged volume distance, and r_d represents the sound horizon at the baryon drag epoch. The anisotropic BAO measurements encompass $D_M(z)/r_d$ and $D_H(z)/r_d$, where $D_M(z)$ denotes the comoving angular diameter distance and $D_H(z)$ is expressed as $c/H(z)$, indicating the Hubble distance. These measurements, at eight different effective redshifts, have been derived from the extensive observations conducted by the SDSS collaboration and continuously refined over the past 20 years [2]. We refer to this dataset as BAO. In some analyses, we also consider the partial dataset of 7 BAO measurements with redshift $z > 0.8$ from Table I, referred to as BAO($z > 0.8$). As demonstrated in [91,92], the constraints derived from the

TABLE I. Clustering measurements for each of the BAO samples from SDSS Ref. [2] and DES Y6 [93].

Parameter	z_{eff}	$D_{\text{V}}(z)/r_{\text{d}}$	$D_{\text{M}}(z)/r_{\text{d}}$	$D_{\text{H}}(z)/r_{\text{d}}$
MGS	0.15	4.47 ± 0.17	$\cdots$	$\cdots$
BOSS Galaxy	0.38	$\cdots$	10.23 ± 0.17	25.00 ± 0.76
BOSS Galaxy	0.51	$\cdots$	13.36 ± 0.21	22.33 ± 0.58
eBOSS LRG	0.70	$\cdots$	17.86 ± 0.33	19.33 ± 0.53
eBOSS ELG	0.85	$18.33^{+0.57}_{-0.62}$	$\cdots$	$\cdots$
DES Y6 BAO	0.85	$\cdots$	19.51 ± 0.41	$\cdots$
eBOSS Quasar	1.48	$\cdots$	30.69 ± 0.80	13.26 ± 0.55
Lyα-Lyα	2.33	$\cdots$	37.6 ± 1.9	8.93 ± 0.28
Lyα-Quasar	2.33	$\cdots$	37.3 ± 1.7	9.08 ± 0.34

individual high-z and low-z BAO datasets yield noticeably different correlations in the H_0-Ω_{m} plane. Given that the correlation in this plane is crucial for elucidating the H_0 tension, we opted to limit our BAO sample to redshifts greater than 0.8. Additionally, we included the data point $D_{\text{M}}(z)/r_{\text{d}} = 19.51 \pm 0.41$ at $z_{\text{eff}} = 0.85$ obtained with the BAO feature from galaxy clustering in the completed Dark Energy Survey (DES), consisting of six years (Y6) of observations [93].

(iii) SNe Ia: We incorporate the most recent SH0ES Cepheid host distance anchors [10] into the likelihood function by integrating distance modulus measurements of SNe Ia taken from the Pantheon+ sample [94]. The 1701 light curves in the Pantheon+ dataset correspond to 1550 different SNe Ia events over the redshift range $z \in [0.001, 2.26]$. We refer to this dataset as PP&SH0ES.

(iv) Cosmic Shear: We use KiDS-1000 data [95,96], which include the weak lensing two-point statistics data for both the auto and cross-correlations across five tomographic redshift bins [97]. We employ the public likelihood in KiDS-1000 MontePython likelihood, and follow the KiDS team analysis, adopting the COSEBIs (Complete Orthogonal Sets of E/B-Integrals) likelihood in our analysis [4]. For the prediction of the matter power spectrum, we use the augmented halo model code, HMcode [98]. We highlight that at the level of linear perturbation theory and Boltzmann equations, Λ_{s}CDM has the same shape as predicted by ΛCDM. The only effect on the matter power spectrum comes from the $H(z)$ behavior at late times. As HMcode is robustly tested at the percent level for variations in $H(z)$ functions beyond ΛCDM, we conclude that no further change to HMcode is necessary to apply cosmic shear measurements on Λ_{s}CDM. On the other hand, for Λ_{s}VCDM, we highlight that at the level of linear perturbation theory and Boltzmann equations, the model described here is well-modeled, in the sense that the theory possesses a Lagrangian leading to

unique evolution once the background evolution is given. Furthermore, as discussed in [38], Λ_{s}VCDM does not change the behavior of the spatial components of the Einstein equations, i.e., the lensing equation, for the two gravitational potentials. Λ_{s}VCDM will affect the time-time component of the field equations, but we expect these effects to be prevalent only on large scales. Since the theory is minimal by construction, the auxiliary field does not propagate, preventing it from becoming unstable. In the small-scale regime, all no-ghost conditions for both matter fields are trivially satisfied. Therefore, we can use the same nonlinear scale results found in GR and its minimal variation as implemented by default in the HMcode model. We refer to this dataset as KiDS-1000.

IV. RESULTS AND DISCUSSION

The marginalized 68% CL constraints on the baseline free parameters and selected derived parameters for the Λ_{s}CDM, Λ_{s}VCDM, and ΛCDM models are presented in Table II. The Planck, BAO, and PP&SH0ES datasets are utilized in different combinations of interest. Figures 1–3 show the one- and two-dimensional marginalized distributions for a few parameters of interest of the models considered in this work, derived from Planck only dataset, and its combinations with PP&SH0ES, BAO ($z > 0.8$), and the full BAO dataset.

As a primary feature of our observational tests, it is notable that the six parameters of the common baseline remain unchanged across all models, with the maximum shift of $\sim 1\sigma$ between Λ_{s}VCDM and ΛCDM. When interpreting in terms of derived quantities from these core parameters, it becomes evident that since both scenarios (Λ_{s}CDM and Λ_{s}VCDM) can produce a high value for H_0, they simultaneously will project a lower value for Ω_{m} compared to the ΛCDM model. This is because the CMB accurately measures $\Omega_{\text{m}}h^2$ from the peak structure of the damping tail, resulting into a negative correlation in the H_0-Ω_{m} plane. This trend is observed in all analyses carried out, but the effect is more evident in the analysis with CMB only. Previous studies [30–33] (see also [58]) have shown that these models provide a compelling alternative solution to the H_0 tension.

The effects on CMB anisotropies are anticipated to be observed in the amplitude of the late integrated Sachs-Wolfe (ISW) effect, particularly manifested at large angular scales. This effect hinges on the duration of the dark energy-dominated stage, determined by the time of equality between matter and dark energy density, fixed by the ratio $\Omega_{\Lambda_{\text{s}}}/\Omega_{\text{m}}$, where $\Omega_{\text{m}} = \Omega_{\text{b}} + \Omega_{\text{cdm}}$. A higher $\Omega_{\Lambda_{\text{s}}}$ suggests an extended dark energy domination period, consequently amplifying the late ISW effect. In our primary baseline, constraints on the baryon density are expected to remain practically unchanged. Additionally, in the models under

TABLE II. Marginalized constraints (mean values with 68% CL limits) for the free and selected derived parameters of the Λ_sCDM, Λ_sVCDM, and ΛCDM models across different dataset combinations. The relative best fit $\Delta\chi^2_{\min}$, Akaike information criterion ΔAIC, and log-Bayesian evidence $\Delta\ln\mathcal{Z}$ are also provided; negative values indicate a preference for the Λ_sCDM/Λ_sVCDM models over the standard ΛCDM model.

Dataset	Planck	Planck+BAO(z>0.8)	Planck+BAO	Planck +PP&SH0ES	Planck+BAO(z>0.8) +PP&SH0ES	Planck+BAO +PP&SH0ES
Model	Λ_sCDM	Λ_sCDM	Λ_sCDM	Λ_sCDM	Λ_sCDM	Λ_sCDM
	Λ_sVCDM	Λ_sVCDM	Λ_sVCDM	Λ_sVCDM	Λ_sVCDM	Λ_sVCDM
	ΛCDM	ΛCDM	ΛCDM	ΛCDM	ΛCDM	ΛCDM
$10^2\omega_b$	2.241 ± 0.015	2.243 ± 0.015	2.237 ± 0.014	2.246 ± 0.015	$2.245^{+0.015}_{-0.013}$	$2.245^{+0.015}_{-0.013}$
	2.250 ± 0.015	2.243 ± 0.015	2.236 ± 0.014	2.246 ± 0.015	2.249 ± 0.014	2.244 ± 0.014
	2.238 ± 0.014	2.245 ± 0.015	2.244 ± 0.014	2.264 ± 0.014	2.267 ± 0.014	2.262 ± 0.013
ω_{cdm}	0.1195 ± 0.0012	0.1193 ± 0.0011	0.1203 ± 0.0010	0.1190 ± 0.0010	0.1192 ± 0.0010	0.1197 ± 0.0010
	0.1185 ± 0.0013	$0.1191^{+0.0012}_{-0.0011}$	0.1203 ± 0.0010	0.1190 ± 0.0011	0.1191 ± 0.0011	0.1198 ± 0.0010
	0.1200 ± 0.0012	0.1189 ± 0.0011	0.1191 ± 0.0009	0.1173 ± 0.0010	0.1168 ± 0.0010	0.1175 ± 0.0008
$100\theta_s$	1.04189 ± 0.00029	1.04192 ± 0.00029	1.04185 ± 0.00028	1.04194 ± 0.00029	1.04198 ± 0.00028	1.04195 ± 0.00029
	1.04201 ± 0.00030	1.04194 ± 0.00030	1.04184 ± 0.00029	$1.04197^{+0.00028}_{-0.00032}$	1.04198 ± 0.00029	1.04190 ± 0.00030
	$1.04190^{+0.00027}_{-0.00031}$	1.04198 ± 0.00029	1.04198 ± 0.00028	1.04217 ± 0.00028	1.04223 ± 0.00028	1.04216 ± 0.00028
$\ln(10^{10}A_s)$	3.040 ± 0.014	$3.041^{+0.011}_{-0.015}$	3.037 ± 0.014	$3.039^{+0.012}_{-0.014}$	$3.039^{+0.013}_{-0.015}$	$3.040^{+0.012}_{-0.014}$
	3.033 ± 0.016	3.036 ± 0.015	3.034 ± 0.014	3.032 ± 0.015	3.034 ± 0.015	3.036 ± 0.014
	3.046 ± 0.014	$3.049^{+0.013}_{-0.015}$	3.048 ± 0.014	$3.058^{+0.015}_{-0.017}$	3.059 ± 0.015	$3.056^{+0.014}_{-0.016}$
n_s	0.9669 ± 0.0043	0.9672 ± 0.0040	0.9645 ± 0.0039	0.9684 ± 0.0039	0.9676 ± 0.0038	0.9663 ± 0.0040
	0.9694 ± 0.0044	0.9678 ± 0.0041	0.9646 ± 0.0035	0.9677 ± 0.0039	0.9677 ± 0.0038	0.9660 ± 0.0038
	0.9657 ± 0.0041	0.9681 ± 0.0039	0.9675 ± 0.0036	0.9722 ± 0.0039	$0.9736^{+0.0036}_{-0.0041}$	0.9720 ± 0.0036
τ_{reio}	0.0528 ± 0.0073	$0.0536^{+0.0059}_{-0.0078}$	0.0509 ± 0.0072	$0.0530^{+0.0060}_{-0.0074}$	$0.0528^{+0.0055}_{-0.0076}$	$0.0527^{+0.0057}_{-0.0071}$
	0.0507 ± 0.0076	0.0514 ± 0.0076	0.0493 ± 0.0071	$0.0498^{+0.0078}_{-0.0069}$	$0.0504^{+0.0079}_{-0.0070}$	0.0504 ± 0.0074
	$0.0550^{+0.0065}_{-0.0072}$	$0.0573^{+0.0066}_{-0.0082}$	$0.0568^{+0.0066}_{-0.0074}$	$0.0630^{+0.0073}_{-0.0087}$	0.0642 ± 0.0079	$0.0620^{+0.0067}_{-0.0084}$
$z_\dagger$	> 1.45 (95% CL)	$2.20^{+0.17}_{-0.38}$	> 2.11 (95% CL)	$1.83^{+0.11}_{-0.19}$	$1.87^{+0.15}_{-0.18}$	$2.31^{+0.15}_{-0.36}$
	$1.88^{+0.28}_{-0.58}$ [> 1.20 (95% CL)]	$2.12^{+0.23}_{-0.27}$	> 2.06 (95% CL)	$1.80^{+0.13}_{-0.18}$	$1.86^{+0.12}_{-0.21}$	$2.20^{+0.16}_{-0.23}$
	-	-	-	-	-	-
H_0[km/s/Mpc]	$70.77^{+0.79}_{-2.70}$	$70.39^{+0.87}_{-1.20}$	$68.92^{+0.46}_{-0.55}$	72.07 ± 0.88	71.68 ± 0.73	69.82 ± 0.49
	$73.40^{+1.80}_{-4.60}$	$70.72^{+0.87}_{-1.30}$	69.10 ± 0.55	72.25 ± 0.91	71.86 ± 0.79	70.01 ± 0.50
	67.39 ± 0.55	67.88 ± 0.51	67.82 ± 0.41	68.69 ± 0.47	68.91 ± 0.46	$68.62^{+0.34}_{-0.38}$
Ω_m	$0.2860^{+0.0230}_{-0.0099}$	$0.2880^{+0.0100}_{-0.0088}$	0.3018 ± 0.0056	0.2738 ± 0.0072	0.2770 ± 0.0063	$0.2929^{+0.0044}_{-0.0051}$
	$0.2650^{+0.0340}_{-0.0190}$	$0.2850^{+0.0110}_{-0.0091}$	0.3001 ± 0.0059	0.2725 ± 0.0073	0.2755 ± 0.0065	0.2915 ± 0.0049
	0.3151 ± 0.0075	0.3083 ± 0.0067	0.3091 ± 0.0054	0.2981 ± 0.0060	0.2952 ± 0.0058	0.2989 ± 0.0046
σ_8	$0.8210^{+0.0064}_{-0.0110}$	$0.8169^{+0.0062}_{-0.0070}$	0.8143 ± 0.0062	0.8228 ± 0.0068	0.8215 ± 0.0067	0.8160 ± 0.0065
	$0.8620^{+0.0160}_{-0.0380}$	$0.8414^{+0.0094}_{-0.0140}$	0.8316 ± 0.0078	0.8560 ± 0.0120	0.8520 ± 0.0110	0.8385 ± 0.0090
	$0.8121^{+0.0055}_{-0.0061}$	0.8098 ± 0.0061	0.8097 ± 0.0058	$0.8085^{+0.0060}_{-0.0070}$	0.8077 ± 0.0062	$0.8085^{+0.0060}_{-0.0067}$
S_8	$0.801^{+0.026}_{-0.016}$	0.800 ± 0.014	0.817 ± 0.010	0.786 ± 0.011	0.789 ± 0.010	$0.806^{+0.009}_{-0.010}$
	$0.808^{+0.021}_{-0.017}$	0.819 ± 0.012	0.832 ± 0.011	0.815 ± 0.011	$0.816^{+0.011}_{-0.012}$	0.826 ± 0.011
	0.832 ± 0.013	0.821 ± 0.012	0.822 ± 0.010	0.806 ± 0.011	0.801 ± 0.011	0.807 ± 0.010
t_0[Gyr]	$13.62^{+0.12}_{-0.04}$	$13.64^{+0.05}_{-0.04}$	$13.70^{+0.03}_{-0.02}$	13.56 ± 0.04	13.58 ± 0.03	13.66 ± 0.03
	$13.52^{+0.18}_{-0.09}$	$13.62^{+0.06}_{-0.04}$	13.69 ± 0.03	13.56 ± 0.04	13.57 ± 0.04	13.65 ± 0.03
	13.79 ± 0.02	13.78 ± 0.02	13.78 ± 0.02	13.75 ± 0.02	13.74 ± 0.02	13.75 ± 0.02
$\chi^2_{\min}$	2778.06	2785.48	2796.16	4082.28	4086.42	4106.24
	2777.36	2782.92	2793.42	4079.60	4086.34	4106.30
	2780.52	2792.14	2797.44	4105.80	4114.24	4122.20
$\Delta\chi^2_{\min}$	-2.46	-6.66	-1.28	-23.52	-27.82	-15.96
	-3.16	-9.22	-4.02	-26.20	-27.90	-15.90
ΔAIC	-0.46	-4.66	0.72	-21.52	-25.82	-13.96
	-1.16	-7.22	-2.02	-24.20	-25.90	-13.90
$\ln\mathcal{Z}$	-1423.17	-1427.41	-1432.97	-2076.65	-2079.93	-2089.64
	-1422.21	-1425.95	-1432.39	-2074.32	-2078.44	-2088.24
	-1424.45	-1429.64	-1433.52	-2088.18	-2092.07	-2096.01
$\Delta\ln\mathcal{Z}$	-1.28	-2.23	-0.55	-11.53	-12.14	-6.37
	-2.24	-3.69	-1.13	-13.86	-13.63	-7.77

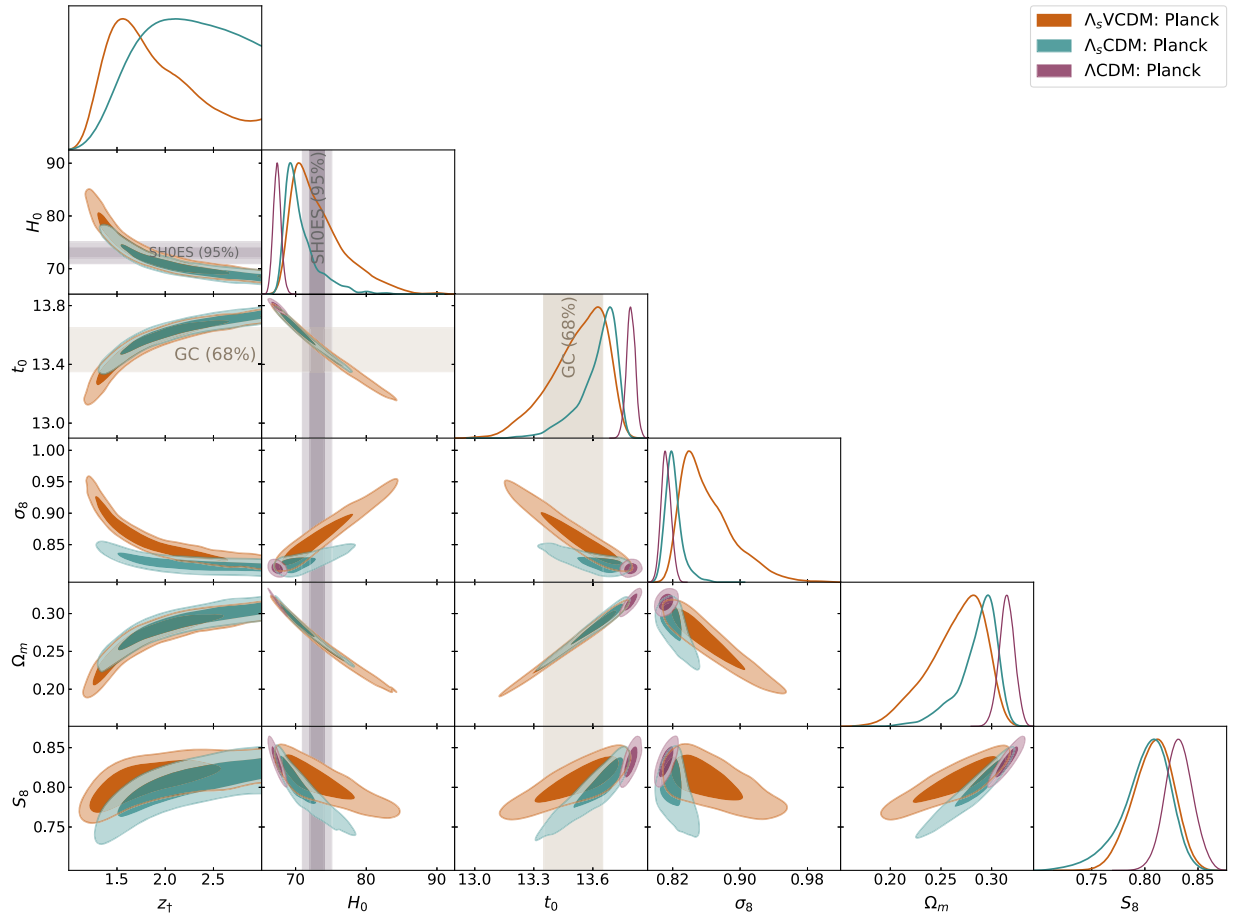FIG. 1. One- and two-dimensional (68% and 95% CL) marginalized distributions of the Λ_sVCDM, Λ_sCDM, and ΛCDM model parameters from Planck. The vertical violet and brown bands show the local measurements of $H_0 = 73.04 \pm 1.04$ km s^{-1} Mpc^{-1} (SH0ES) [10] and $t_0 = 13.50 \pm 0.15$ Gyr (stat.) [99].

consideration, we assume spatial flatness for our Universe. Thus, at late times, $\Omega_{\Lambda_s} = 1 - \Omega_m$ (neglecting radiation), and the alterations induced by different constraints on Ω_{cdm} will primarily govern corrections to CMB anisotropies at large scales. On the other hand, Ω_{cdm} will influence the amplitude of the third peak in the CMB power spectra and also impact constraints on H_0 through the relationship $h \simeq \sqrt{\omega_m/(1 - \Omega_{\Lambda_s})}$ (assuming $\Omega_k = 0$) at late times. Furthermore, alterations in the late-time expansion of the Universe induced by the mirror AdS-dS transition will modify the angular diameter distance at decoupling. The magnitude of these correlations in H_0 is directly proportional to the potential values for the mirror AdS-dS transition (see Fig. 2 and explanation in [30]). Due to the significant degeneracy and correlation between $z_\dagger$ and H_0, we conclude that the CMB data alone has limited constraining power for directly determining the transition redshift $z_\dagger$. Therefore, it is imperative to complement CMB data with geometric measurements to achieve a comprehensive understanding of $z_\dagger$.

Furthermore, we can interpret these results in a physical context, stemming from a fundamental property of the model: a transition from anti–de Sitter to de Sitter dynamics at a redshift of $z_\dagger \sim 2$. For the Λ_sVCDM model, following the AdS-dS transition, the introduction of a new auxiliary scalar field results in an effective cosmological constant, leading to a prediction that its density parameter surpasses that of the ΛCDM model, i.e., $\Omega_{\Lambda_s} > \Omega_\Lambda$ after transition. Consequently, assuming that the density evolution of other species such as baryons and radiation remains unaffected, this also implies that the cold dark matter density will dilute at a faster rate than expected, thereby predicting lower values for Ω_m as summarized in Table II. Then, as the transition indicates a greater influence of effective dark energy and a decrease in cold dark matter density at late times, the expected consequence is that the Hubble parameter, $H(z)$, will be greater than predicted in the ΛCDM model. In other words, the Universe expands faster in the Λ_sVCDM model after the transition than in the ΛCDM model. The interpretation of parameters and dynamics for the Λ_sCDM model is the same; however, the transition
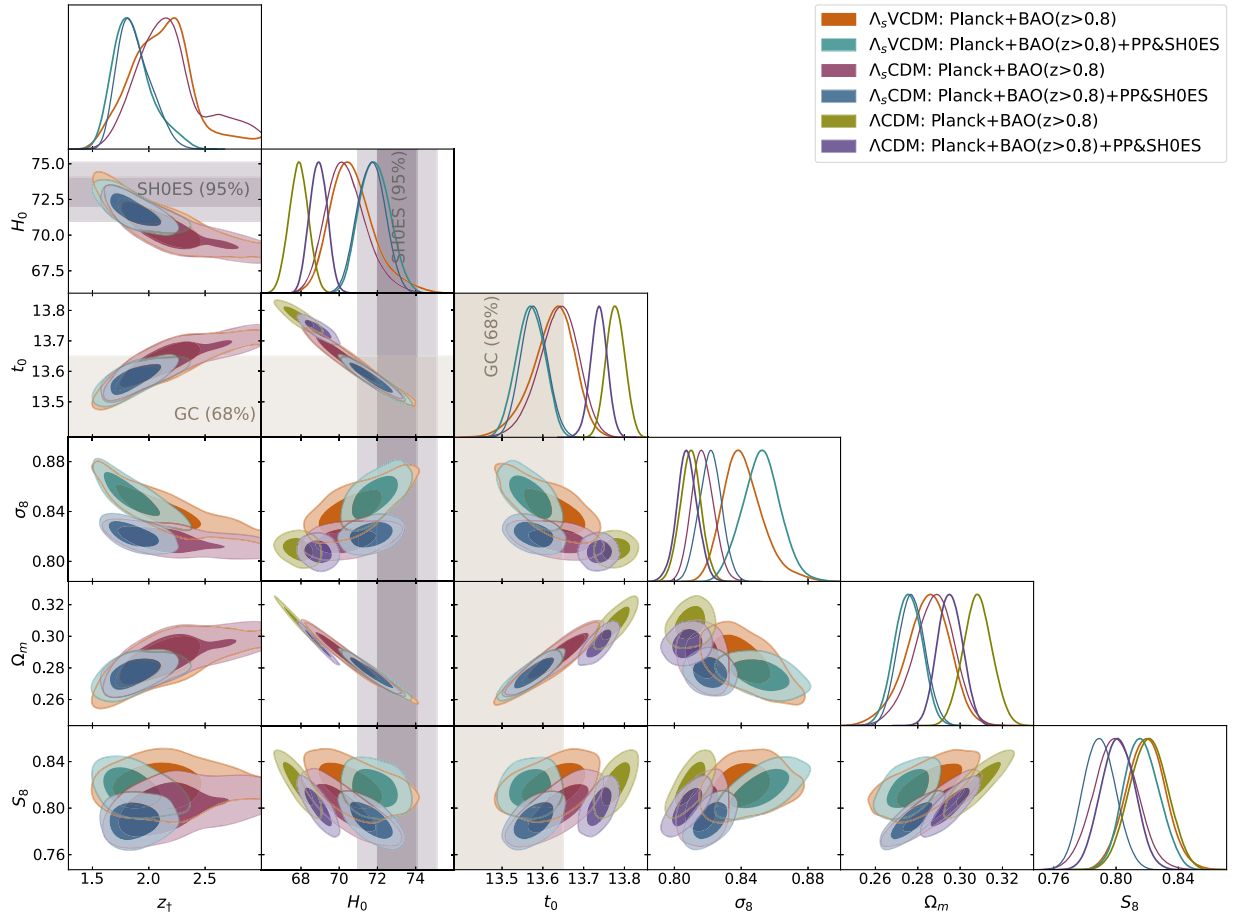
FIG. 2. One- and two-dimensional (68% and 95% CL) marginalized distributions of the Λ_sVCDM, Λ_sCDM, and ΛCDM model parameters from Planck + BAO($z > 0.8$) and Planck + BAO($z > 0.8$)+ PP&SH0ES. The vertical violet and brown bands show the local measurements of $H_0 = 73.04 \pm 1.04$ km s^{-1} Mpc^{-1} (SH0ES) [10] and $t_0 = 13.50 \pm 0.15$ Gyr (stat.) [99].

occurs instantaneously in this scenario. It is worth noting that both models predict a transition redshift $z_\dagger$ consistent with each other in all analyses conducted.

It is interesting to notice the difference in the results for H_0 between Λ_sCDM and Λ_sVCDM in the constraints derived solely from Planck data. At the background level, they differ slightly since the transition is smooth, although rapid, for the Λ_sVCDM model. However, at the level of perturbations, the Bardeen potential Φ changes because its dynamics depends on $a\Lambda_{s,a}$, which can assume large values.[3]

This will also affect the dynamics of δ_m, which explicitly depends on $\dot{\Phi}$. This combination of changes leads to differences between the Λ_sCDM and Λ_sVCDM models, allowing the latter to have larger contours and a mean value for H_0 closer to the SH0ES measurement of $H_0 = 73.04 \pm 1.04$ km s^{-1} Mpc^{-1} [10].[4] Another way to understand this larger value for H_0 is to realize that $z_\dagger$ tends to be smaller in the Λ_sVCDM model compared to the Λ_sCDM model. Notably, for Λ_sVCDM in the Planck-alone case, the lower bound on $z_\dagger$ reaches values of 1.2 at a 95% CL (compared to 1.45 in the Λ_sCDM model), leading to large values of H_0 (and thereby, smaller values of Ω_m). When the

---

[3]The equations of motion governing the dynamics for Φ can be written as $\Phi_{,\tau} + aH\Psi = \frac{3}{2}(a^2/k^2)\Gamma\sum_I(\varrho_I + p_I)\theta_I$, where τ is the conformal time, Ψ is the second Bardeen potential, and θ_I corresponds to the scalar component of the Ith fluid 3-velocity, I running over all the standard matter fields. Here $\Gamma \equiv [k^2/a^2 - 3H_{,\tau}/a]/[k^2/a^2 + (9/2)\sum_K(\varrho_K + p_K)]$. Since we can rewrite Γ as $\Gamma \equiv [k^2/a^2 + (9/2)\sum_K(\varrho_K + p_K) - (a/2)\Lambda_{s,a}]/[k^2/a^2 + (9/2)\sum_K(\varrho_K + p_K)]$, we can deduce a suppression of the numerator at transition (or even a switch of its sign for a very sharp transition). In Λ_sCDM, having set the perturbation dynamics identical to GR, Γ is unity.

[4]To disentangle these two contributions—the one of the background from the one of the modified perturbation equations—it could be interesting to modify the background of Λ_sCDM exactly match that of Λ_sVCDM, smoothing out the instantaneous transition into a smooth but rapid one. Then we could see how much the smoothing of the background improves the fit of Λ_sCDM, and vice versa, how much the modified perturbation dynamics of Λ_sVCDM affect the results. We leave the discussion of this point for a separate project.
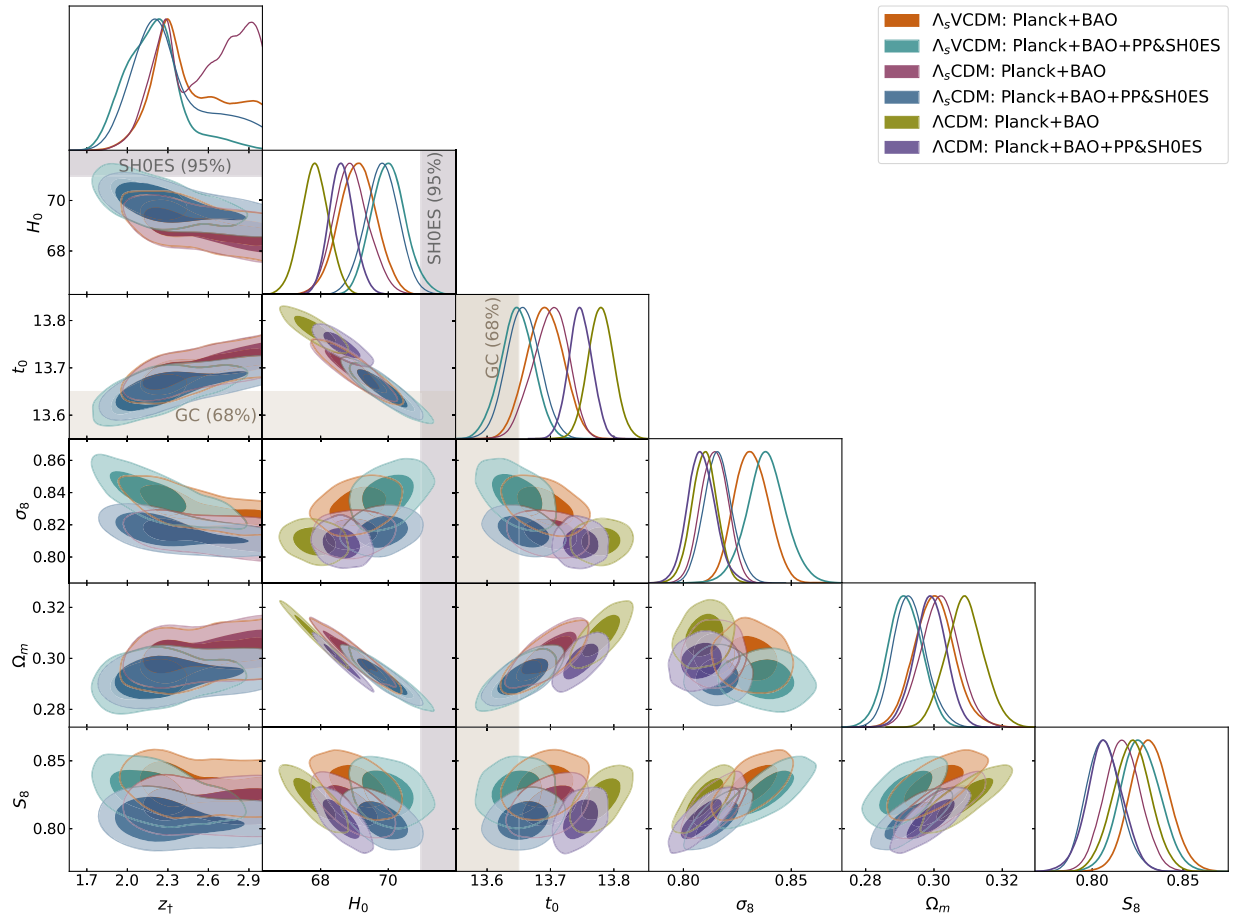
FIG. 3.   One- and two-dimensional (68% and 95% CL) marginalized distributions of the Λ_sVCDM, Λ_sCDM, and ΛCDM model parameters from Planck + BAO and Planck + BAO+ PP&SH0ES. The vertical violet and brown bands show the local measurements of $H_0 = 73.04 \pm 1.04$ km s^{-1} Mpc^{-1} (SH0ES) [10] and $t_0 = 13.50 \pm 0.15$ Gyr (stat.) [99].

models become indistinguishable from the ΛCDM model at the high end of $z_\dagger$, they predict H_0 values similar to those of the ΛCDM. This picture places H_0 in the range of 75.2 km s^{-1} Mpc^{-1} to 68.8 km s^{-1} Mpc^{-1}, with a mean value of 73.4 km s^{-1} Mpc^{-1}. This constraint aligns perfectly with the SH0ES measurement of 73.30 ± 1.04 km s^{-1} Mpc^{-1} (derived by including high-z SN Ia) [10], with the mean value almost exactly matching it, and with the latest measurements of 73.17 ± 0.86 km s^{-1} Mpc^{-1} [11] and 73.22 ± 0.68(stat) ± 1.28(sys) km s^{-1} Mpc^{-1} [100]. Notably, H_0 predictions from the Planck-alone analysis of both Λ_sCDM and Λ_sVCDM models exhibit no tension at all with any of the SH0ES measurements. Specifically, the discrepancy for Planck-Λ_sCDM is only $1 - 1.2\sigma$, and for Planck-Λ_sVCDM, it is almost nonexistent, at an amazingly low $0.0 - 0.1\sigma$.

Next, we examine the ramifications of our choices within the BAO sample when considering both Λ_sCDM and Λ_sVCDM. In the joint analysis involving Planck + BAO ($z > 0.8$, including DES Y6), a clear trend emerges toward

lower values of $\Omega_m \sim 0.29$, consequently leading to higher values of $H_0 \sim 70.4$–70.7 km s^{-1} Mpc^{-1}. This trend is attributed to the distinctive correlation exhibited by the BAO sample within this redshift range [2]. In this context, the cosmological framework's capability to anticipate these correlations naturally manifests in this joint analysis. Expanding our scope to encompass all BAO samples, i.e., Planck + BAO, the comprehensive sample unsurprisingly aligns the BAO constraints more closely with the values prescribed by the ΛCDM model. However, it is noteworthy that both models still predict $H_0 \sim 69$ km s^{-1} Mpc^{-1}, values slightly higher than those predicted by the ΛCDM model, thereby reducing the H_0 tension. Consequently, our analysis solely with Planck + BAO helps in mitigating the H_0 tension. From these joint analyses, evaluating the tension individually using the standard 1D tension metric, we find a tension of $\sim 1.8\sigma$ for both models from Planck + BAO($z > 0.8$) and a tension of $\sim 3.3\sigma$ from Planck + BAO. While for the combination Planck + BAO($z > 0.8$), we can constrain
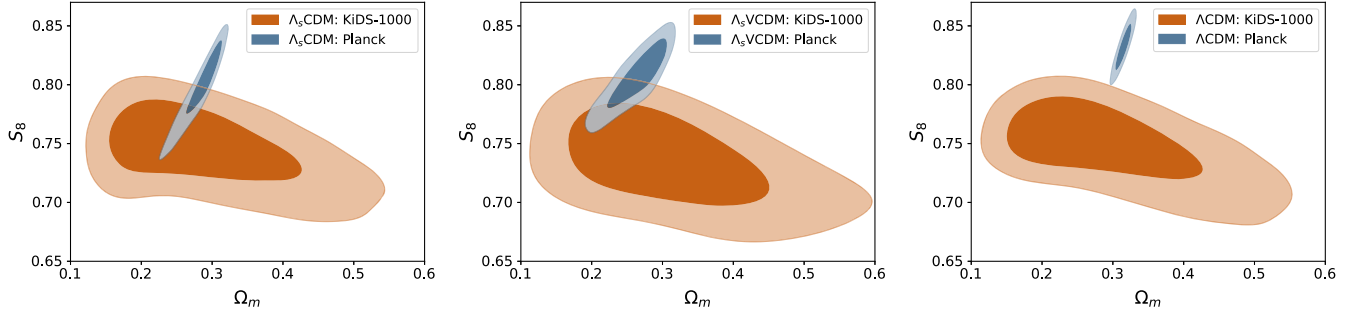
FIG. 4. 2D contours (68% and 95% CL) in the Ω_{m}-S_8 plane for Λ_{s}CDM, Λ_{s}VCDM, and ΛCDM. $S_8 = 0.746^{+0.026}_{-0.021}$ (Λ_{s}CDM: KiDS-1000), $S_8 = 0.801^{+0.026}_{-0.016}$ (Λ_{s}CDM: Planck), $S_8 = 0.736 \pm 0.027$ (Λ_{s}VCDM: KiDS-1000), $S_8 = 0.808^{+0.021}_{-0.017}$ (Λ_{s}VCDM: Planck), $S_8 = 0.749^{+0.027}_{-0.020}$ (ΛCDM: KiDS-1000), $S_8 = 0.832 \pm 0.013$ (ΛCDM: Planck) at 68% CL. In the Λ_{s}CDM and Λ_{s}VCDM models, the S_8 tension reduces to significance levels of 1.7σ and 2.2σ, respectively, compared to a higher level of 3.0σ in the standard ΛCDM model.

$z_\dagger \sim 2.1$–2.2 at 68% CL, when we consider the full BAO data, we find only a lower limit that gives $z_\dagger > 2.1$ at 95% CL for both Λ_{s}CDM and Λ_{s}VCDM.[5]

We further investigated the combination of the PP&SH0ES and Planck datasets. The findings are summarized in Table II. Consistent with previous analyses, both Λ_{s}CDM and Λ_{s}VCDM models yield observational constraints that align well with each other in this combined assessment. Employing the standard 1D tension metric to assess individual tensions, we observe a tension of approximately 0.6σ on H_0, with $H_0 \sim 72 \ \mathrm{km\,s^{-1}\,Mpc^{-1}}$. Consequently, based on this joint analysis, we conclude that both models effectively alleviate the tension in H_0 with significant statistical support. It is noteworthy that, as it is well known, the Planck data and PP&SH0ES data are in tension within the ΛCDM model. Therefore, combining these two datasets for the ΛCDM analyses is not statistically worthwhile, but these results are given here for completeness. The same argument applies to Planck+ PP&SH0ES baseline and Planck + BAO; consequently, combining all these datasets is not statistically sound in this scenario. However, with regards to the BAO samples, we

can instead only consider the combination of Planck + BAO($z > 0.8$)+ PP&SH0ES, as these datasets demonstrate internal consistency, i.e., these exhibit no tension among them. The results of our analysis involving Planck + BAO($z > 0.8$)+ PP&SH0ES are also summarized in Table II. In this case, we observe only a tension of approximately 1σ between the predictions of Λ_{s}CDM and Λ_{s}VCDM and the SH0ES H_0 measurement. Therefore, based on this comprehensive joint analysis, we can conclude that both models effectively alleviate the H_0 tension.

We now turn our attention to the weighted amplitude of matter fluctuations, quantified by the parameter $S_8 = \sigma_8 \sqrt{\Omega_{\mathrm{m}}/0.3}$ using the standard definition. Initially, it is crucial to acknowledge that in all joint analyses, both the Λ_{s}CDM and Λ_{s}VCDM models exhibit a tendency to project higher values for σ_8 compared to ΛCDM, with Λ_{s}VCDM notably predicting a higher value compared to Λ_{s}CDM. This difference arises from the fact that Λ_{s}VCDM incorporates linear perturbative effects of scalar modes, whereas the Λ_{s}CDM model does not. Fundamentally, this distinction arises from the analysis of CMB data, where Λ_{s}VCDM also impacts the CMB spectrum during late times, i.e., at large angular scales. This influence stems from alterations in the scalar fields Φ and Ψ, their temporal variations, and the background evolution. Consequently, with respected to the standard ΛCDM model, Λ_{s}VCDM affects the CMB spectrum in two distinct ways, whereas Λ_{s}CDM solely influences it through background evolution $H(z)$. Conversely, as discussed previously, it is established that both models predict a lower value for Ω_{m}. In other words, both the Λ_{s}VCDM and Λ_{s}CDM models forecast an increased rate of structure formation, yet simultaneously anticipate less matter density parameter today, resulting in overall lower values for S_8 compared to ΛCDM. It is noteworthy that all constraints on S_8 are mutually compatible at approximately $\sim 1\sigma$ CL between Λ_{s}VCDM and Λ_{s}CDM.

To correctly assess the S_8 tension between the weak lensing measurements and the CMB ones, we conducted an

---

[5]Recent BAO measurements from the DESI collaboration [7,101,102] have become available, offering potentially new insights into the nature of dark energy. While the completed SDSS-BAO dataset (BOSS + eBOSS) [2] used in this study has a constraining power comparable to the DESI-BAO dataset [7], the DESI data may provide fresh evidence regarding the dynamical aspects of dark energy (see, e.g., [103–108]). However, the models considered in this paper do not account for dynamical dark energy in their background evolution. The sole free parameter in these theories, the transition epoch $z_\dagger$, is already well-constrained by the complete SDSS-BAO dataset. Consequently, incorporating the DESI data is not expected to significantly alter the precision of the baseline parameters or their correlations relative to the SDSS sample. Therefore, our conclusions remain robust even when DESI data are considered. In a future study, we will update the results using the BAO-DESI dataset for performance evaluation purposes. However, the main results and conclusions are anticipated to remain consistent with those presented here.

analysis using only KiDS-1000 data [4,96] for all the models under consideration because the S_8 constraints are model-dependent for this observable. Figure 4 illustrates the 2D contour plots in the S_8-Ω_m plane for the Λ_sCDM, Λ_sVCDM, and ΛCDM models. In each case, the figure compares the 2D contours between Planck and KiDS-1000 data exclusively for that particular model. As widely recognized, the right panel displays a disagreement in the S_8-Ω_m plane for the ΛCDM model between the two probes, indicating an S_8 tension at the 3.0σ level. Conversely, in the left panel depicting the Λ_sCDM scenario, we observe strong compatibility between the bounds in the S_8-Ω_m plane from Planck and KiDS-1000 data considered separately. In this scenario, we derive $S_8 = 0.746^{+0.026}_{-0.021}$ at 68% CL from the KiDS-1000 sample, while considering the Planck analysis alone, we observe $S_8 = 0.801^{+0.026}_{-0.016}$. Subsequently, we find that the tension between both samples amounts to approximately 1.7σ. We arrive at similar conclusions for the Λ_sVCDM model, as shown in the middle panel. We note that both the Λ_sVCDM and Λ_sCDM models do not significantly alter the KiDS-1000 alone constraints in the S_8-Ω_m plane compared to ΛCDM. These models affect the three two-point correlation functions (3×2pt analysis) by primarily altering the background evolution described by $H(z)$, though Λ_sVCDM predicts changes at the linear level of order 1; however, these effects are not significantly distinguishable from those in ΛCDM. As established in the literature, cosmic shear analyses alone are unable to effectively constrain H_0 and Ω_m simultaneously, but they do constrain the parameter σ_8. Consequently, the constraints in Λ_sCDM are expected to be nearly identical to those in ΛCDM, as both models are virtually indistinguishable at the level of σ_8. Therefore, cosmic shear alone will not differentiate the constraints on H_0 and Ω_m between these two models. On the other hand, as shown in Table II, the Λ_sVCDM model, in addition to altering the constraints on Ω_m, also predicts changes in σ_8 due to minimal differences in linear perturbations compared to the ΛCDM model. In terms of cosmic shear analyses, this introduces an additional degeneracy in Ω_m but keeps the resulting S_8 nearly the same as in ΛCDM. Therefore, we conclude that the extended models considered in this work do not predict significant changes in cosmic shear analyses. Thus, the improvement in the S_8 tension in these models essentially arises from modifications in the CMB constraints, which lower the value of S_8 to align with predictions from cosmic shear surveys. Specifically, by reducing Ω_m, as demonstrated in Fig. 1, the positive correlation between the parameters S_8 and Ω_m with $z_\dagger$ results in the observed positive correlation between S_8 and Ω_m in Fig. 4 as well.

The (present-day) age of the universe measured using the oldest globular clusters (GCs), in a model-agnostic way, suggests $t_u = 13.50 \pm 0.15(\text{stat}) \pm 0.23(\text{sys})$ Gyr (± 0.27 with combined uncertainties). This aligns well with the age

predicted by the standard ΛCDM model, though current systematic uncertainties in t_u are substantial. Efforts are underway to reduce these uncertainties to better discriminate among cosmological models through the age they predict, especially those addressing the H_0 tension [109]. Considering only statistical uncertainties, the GC-estimated age shows a $\sim 2\sigma$ tension with ΛCDM in all our analyses summarized in Table II. This level of discrepancy in the age may not indicate a serious issue for many, particularly as long as a model predicts an age of the universe larger than the one from GCs, it remains on the safe side. However, it is important to emphasize that if a cosmological model is promising in resolving the H_0 tension, which directly affects the predicted age, it should not predict an age conflicting with astrophysical estimates such as those from GCs. For instance, the early dark energy (EDE) model, one of the most popular proposals for resolving the H_0 tension, typically not only worsens the S_8 tension but also predicts the age of the universe to be significantly smaller than the ΛCDM prediction, even smaller than GC estimates [110,111]. For example, the axion-like EDE, a prominent EDE model, predicts $t_u = 13.17^{+0.14}_{-0.15}$ Gyr (Planck + SH0ES), which is in $\sim 2\sigma$ tension with the age derived from GCs [110–112]. On the other hand, both Λ_sCDM and Λ_sVCDM models predict an age slightly less than ΛCDM, showing a tension of less than $\sim 1\sigma$ (largest $\sim 1.2\sigma$ in the case of Planck + BAO) in most of our analyses; see Table II and Figs. 1–3. While the age discrepancies between the ΛCDM and EDE predictions and GC measurement alone may not seem significant, an astonishing finding in our analyses of both Λ_sCDM and Λ_sVCDM models is that we reduce the H_0 tension more, the closer the predicted age of the universe gets to the one from GCs. Notably, in the Planck-alone analysis of the Λ_sVCDM, the predicted H_0 and t_0 values exhibit no tension at all, only $\sim 0.1\sigma$ when considering the SH0ES H_0 measurement and the astrophysical age measurement from the oldest GCs.

Having finalized our main statistical and cosmological interpretations, we aim to quantify the (dis)agreement between the models and the observational data used. To this end, we perform a statistical comparison of the extended models, Λ_sCDM and Λ_sVCDM, with the ΛCDM model using the Akaike information criterion (AIC) and log-Bayesian evidence, along with $\chi^2_{\min} = -2\ln\mathcal{L}_{\max}$, where $\mathcal{L}_{\max}$ being the maximum likelihood,[6] as presented in Table II. Specifically, we first present the relative best fit ($\Delta\chi^2_{\min} = \chi^2_{\min,\Lambda_s(\text{V})\text{CDM}} - \chi^2_{\min,\Lambda\text{CDM}}$) and the relative AIC ($\Delta\text{AIC} = \text{AIC}_{\Lambda_s(\text{V})\text{CDM}} - \text{AIC}_{\Lambda\text{CDM}}$, where $\text{AIC} \equiv \chi^2_{\min} + 2N$, with N being the number of free parameters, which serves as the penalization term), both

---

[6]Here, the maximum likelihood is not the mathematical maximum of the likelihood function but rather the maximum likelihood value found in the chains. The same consideration applies to the minimum of χ^2.

defined with respect to the ΛCDM model. The preferred model is the one with the smaller AIC value, with negative values of ΔAIC indicating support for the extended models over ΛCDM, and more negative values indicating stronger support. By convention, significance of support is judged according to the Jeffreys' scale, which rates ΔAIC > 5 as "strong" and ΔAIC > 10 as "decisive" support in favor of the model with the smaller AIC value, regardless of the properties of the models under comparison [113]. We also compute the relative log-Bayesian evidence $\Delta \ln \mathcal{Z} \equiv \ln \mathcal{B}_{ij} = \ln \mathcal{Z}_{\Lambda\text{CDM}} - \ln \mathcal{Z}_{\Lambda_s(\text{V})\text{CDM}}$ (where $\mathcal{B}_{ij} = \mathcal{Z}_i / \mathcal{Z}_j$ is the Bayes' factor with $\mathcal{Z}_i$ and $\mathcal{Z}_j$ being the Bayesian evidences for models i and j, respectively) to assess the evidence for the extended models relative to ΛCDM, using the publicly available package MCEvidence[7] [114,115]. We follow the convention of assigning a negative value when the extended model, either Λ_sCDM or Λ_sVCDM, is preferred over ΛCDM, or vice versa. As with the relative AIC, negative values of $\Delta \ln \mathcal{Z}$ imply support for the extended models over ΛCDM, with more negative values indicating stronger support. We interpret the results using the revised Jeffreys' scale by Trotta [116,117]; the evidence is classified as inconclusive if $0 \le |\ln \mathcal{B}_{ij}| < 1$, weak if $1 \le |\ln \mathcal{B}_{ij}| < 2.5$, moderate if $2.5 \le |\ln \mathcal{B}_{ij}| < 5$, strong if $5 \le |\ln \mathcal{B}_{ij}| < 10$, and very strong if $|\ln \mathcal{B}_{ij}| \ge 10$.

Comparing the Λ_sCDM and Λ_sVCDM models against the standard ΛCDM model in Table II, we observe that both extended models consistently outperform ΛCDM, as indicated by negative values of $\Delta\chi^2_{\min}$, ΔAIC, and $\Delta \ln \mathcal{Z}$ across various datasets. These negative values suggest a preference for the extended models over ΛCDM, with the Λ_sVCDM model generally showing slightly stronger evidence and support compared to Λ_sCDM, though the differences are typically marginal. In particular, $\Delta\chi^2_{\min}$ is negative in all cases, indicating a preference for the extended models. For ΔAIC, the extended models also show negative values, reaffirming this preference, with one exception, though statistically insignificant, in the Planck + BAO dataset for Λ_sCDM, which exhibits a slightly positive value (ΔAIC = 0.7). For the Planck and Planck + BAO datasets, all three models perform similarly. However, with the Planck + BAO($z > 0.8$) dataset, the Λ_sVCDM model receives strong support with ΔAIC = -7.2, while the Λ_sCDM model barely achieves strong support with ΔAIC = -4.7. When including PP&SH0ES data, support for both extended models strengthens significantly, reaching decisive levels. Specifically, the preference for both extended models reaches the significance level of approximately -26 with the Planck + BAO($z > 0.8$)+ PP&SH0ES dataset and around -14 with the full data, viz., the Planck + BAO+ PP&SH0ES combination. The Λ_sVCDM model shows

stronger preference with a ΔAIC value of -24.2, compared to Λ_sCDM, which has a ΔAIC value of -21.5 in the case of Planck+ PP&SH0ES. These findings are further supported by Bayesian evidence. In all cases, $\Delta \ln \mathcal{Z}$ is negative, favoring the extended models. Specifically, we find weak evidence for both extended models in the Planck alone analysis. In the case of Planck + BAO, the evidence remains weak for Λ_sVCDM, while it is inconclusive for Λ_sCDM. On the other hand, the evidence strengthens to weak for Λ_sCDM and to moderate for Λ_sVCDM when using the Planck + BAO($z > 0.8$) dataset. Including PP&SH0ES data significantly improves the evidence for both extended models. We find very strong evidence for both extended models with the Planck+ PP&SH0ES and Planck + BAO($z > 0.8$)+ PP&SH0ES datasets, and strong evidence for the full data, viz., the Planck + BAO+ PP&SH0ES combination. Notably, the Λ_sVCDM model generally shows slightly stronger evidence and support compared to Λ_sCDM. Thus, from a statistical standpoint, a rapid mirror AdS-dS transition in the late universe, viz., at $z \sim 1.8$–2.2, as suggested by the Λ_sVCDM and Λ_sCDM models, performs similarly in explaining the cosmological data and presents a robust alternative to the usual dS-like cosmological constant of the standard ΛCDM model.

To provide insights into the kinematics of the universe in different scenarios, in Fig. 5, we illustrate the comoving Hubble parameter (upper panel), $\dot{a} = H(z)/(1 + z)$ (a dot represents a derivative with respect to the cosmological time), Hubble parameter $H(z)$ (middle panel), and the time rate of change of the Hubble parameter (lower panel), $\dot{H}(z)$, scaled by $3H^2(z)$ for the Planck + BAO($z > 0.8$)+ PP&SH0ES joint analysis. For the Λ_sCDM and Λ_sVCDM scenarios, the panels are produced by doing a weighted sampling from our MCMC chains and plotting for the sampled points using the FGIVENX [118] package; the more frequent the lines, the more probable. For the ΛCDM model, the best-fit prediction from the same joint analysis is shown. Similarly, to provide insights into the dynamics of the sign-switching cosmological constant, Λ_s, particularly regarding the mirror AdS-dS transition epoch, in Fig. 6, we plot the corresponding energy density $\rho_{\Lambda_s}(z)$ scaled by the present-day critical energy density $\rho_{c0} = 3H_0^2$ and the density parameter for both Λ_sCDM (with an abrupt transition) and the Λ_sVCDM (with a smooth transition) models.[8] For Λ_sCDM, we observe an abrupt (instantaneous) lift in the value of the comoving Hubble parameter by yielding a Dirac-delta distribution at the mirror AdS-dS

---

[8]Note that the variations in the posteriors for $\rho_{\Lambda_s}/\rho_{c0}$ at $z = 0$ (corresponding to $\Omega_{\Lambda_s} \approx 1 - \Omega_{\rm m}$ at $z = 0$), due to the small errors in $\Omega_{\rm m}$, are not clearly visible given the range of the y-axis from -1 to 1. A similar situation is observed in the middle and bottom panels of Fig. 5 and the bottom panel of Fig. 6. In contrast, the top panel of Fig. 5, which at $z = 0$ corresponds to H_0, shows visible variations in the posteriors despite the percent-level constraints on H_0, due to the narrower range of the y-axis.
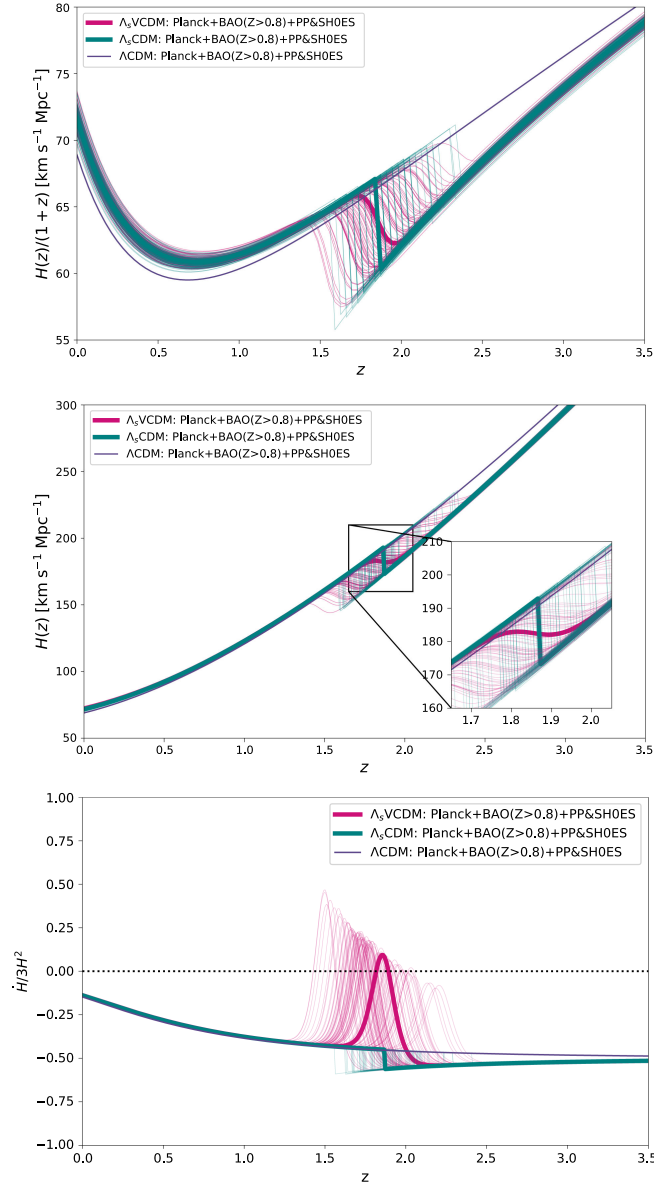
FIG. 5.   Redshift evolution of the comoving Hubble parameter, $\dot{a} = H(z)/(1 + z)$, Hubble parameter, $H(z) = \frac{\dot{a}}{a}$, and the time rate of change of the Hubble parameter scaled by $3H^2$, $\dot{H}/3H^2 = -\frac{1+z}{3H(z)}\frac{\mathrm{d}H(z)}{\mathrm{d}z}$, for the Λ_sCDM, Λ_sVCDM, and ΛCDM models. Plotted for the combined Planck + BAO($z > 0.8$)+ PP&SH0ES dataset.

FIG. 6.   Evolution of the energy density corresponding to Λ in the ΛCDM model and Λ_s in Λ_sCDM and Λ_sVCDM models, and density parameters (Ω) in redshift (z). Upper panel: $\rho_{\Lambda_s}(z)/\rho_{c0}$. Lower panel: $\Omega_{\Lambda_s}(z) = \rho_{\Lambda_s}(z)/\rho_c(z)$ and $\Omega_{\mathrm{m}}(z) = \rho_{\mathrm{m}}(z)/\rho_c(z)$. Note the unusual behavior of $\Omega_{\mathrm{m}}(z)$; given that $\Omega_{\mathrm{m}}(z) \approx 1 - \Omega_{\Lambda_s}(z)$, we have $\Omega_{\mathrm{m}}(z) > 1$ for $z > z_\dagger$, as for these redshifts, Λ_s is AdS-like ($\Omega_{\Lambda_s} < 0$).

transition moment. At this transition moment, $\dot{H}$ also exhibits a Dirac-delta distribution (not shown in the plot) resulting in a jump in its value. Namely, Λ_sCDM exhibits a II (sudden) singularity [119] at $z \to z_\dagger$. One may worry that this can have violent consequences on the structures in the universe; however, a recent work [120] demonstrated that its impact on the formation and evolution of cosmic bound structures is negligible. Therefore, the late time mirror AdS-dS transition does not threaten viability of the Λ_sCDM framework, even in the most extreme case, where an abrupt

transition is assumed. For the Λ_sVCDM scenario, we observe a short period of increasing comoving Hubble parameter, indicating a brief period of accelerated expansion ($\ddot{a} > 0$). An important point about the Λ_sCDM framework is that the rapid mirror AdS-dS transition does not necessarily imply a period of increasing $H(z)$, i.e., $\dot{H}(z) > 0$. Of course, in the abrupt Λ_sCDM scenario, we see an instantaneous jump in the value of $H(z)$ at $z = z_\dagger$. However, for the Λ_sVCDM model, which features a rapid but smooth transition, the mean value of $\dot{H}(z)$ barely becomes positive, and there is a region of the parameter space from our constraints where it remains always negative. Thus, the Λ_sCDM framework is not characterized by a rapidly (abruptly as a limiting case) increasing late-time epoch of $H(z)$, but rather by a rapid (abrupt as a limiting case) mirror AdS-dS transition in the late universe, around $z = z_\dagger \sim 2$, compare the middle panel of Fig. 5 with the lower panel of Fig. 6. Additionally, the term *mirror* implies the Λ_s has the same magnitude before and after the AdS-dS transition, whereas, however, as seen in the lower panel of Fig. 6, the density parameter Ω_{Λ_s} abruptly/rapidly

assumes negative values for $z > z_\dagger$, but it also rapidly approaches zero. This explains why the mirror AdS-dS transition most effectively leads to a deviation from the ΛCDM model if it occurs at a lower redshift. Specifically, the Λ_sCDM and Λ_sVCDM models become indistinguishable from the ΛCDM model, given the precision of the currently available data, if the transition occurs too early, say, if $z_\dagger \gtrsim 4$. At this redshift, whether the cosmological constant is negative or positive, the universe is still highly matter dominated. We see that it is strictly $\Omega_m > 1$ before the mirror AdS-dS transition begins, which is expected because $\Omega_{\Lambda_s} < 0$, while $\Omega_m + \Omega_{\Lambda_s} = 1$ as we consider a spatially flat FLRW universe.

We see that there is a parameter space within our constraints where $\dot{H} > 0$ for a brief period of time. Within GR, this would imply the violation of the null energy condition (implying $\rho + p \geq 0$ for a perfect fluid) by the total energy-momentum tensor of the universe (sign-switching cosmological constant + standard matter fields), signaling the presence of ghosts and/or gradient instabilities.[9] However, in the Λ_sVCDM model [38], realizing Λ_sCDM with a smooth AdS-dS transition in a type II minimally modified gravity called VCDM [39], the occurrence of $\dot{H} > 0$ is completely safe. All the gravity (i.e., gravitational waves) and standard matter fields remain always stable.[10] It is a crucial property of VCDM that it does not possess extra (scalar or not) degrees of freedom, which, if they existed, could be unstable [39], rendering VCDM tailor-made for the Λ_sCDM framework.

V. CONCLUSION

We have conducted a study, in light of observational data, focusing on the implementation of Λ_sCDM [29–32] as a full model by embedding it into the framework of VCDM [39], a type II minimally modified gravity theory, as done in a recent work [38]. Our primary aim was to determine whether the phenomenology of Λ_sCDM would be compromised after allowing the cosmological perturbations to undergo a period of rapid mirror AdS-dS transition in the late universe. *A priori*, without a specific model, we cannot predict whether the fit to the data will worsen. The embedding of Λ_sCDM into VCDM, giving rise to what we call here Λ_sVCDM, was implemented because the VCDM theory, by construction, possesses only two tensor degrees of freedom in the gravity sector as in general relativity and gives rise to no new scalars in the particle spectrum. This allows for a rapid transition in the dark energy

component without leading to any instability. In this paper, we have focused on comparing the fit to the data of three different setups, (i) ΛCDM, (ii) Λ_sCDM, and (iii) Λ_sVCDM, to critically evaluate and highlight the potential improvements offered by the new model, Λ_sVCDM.

We have shown that the Λ_sCDM paradigm, through both the Λ_sCDM (assuming GR and an abrupt transition) and Λ_sVCDM (assuming VCDM and a smooth transition), successfully addresses the H_0 and S_8 tensions simultaneously, without causing any inconsistency with astrophysical estimations of the present-day age of the Universe, such as those from the oldest globular clusters.

On the other hand, when comparing these two particular models, namely, Λ_sCDM and Λ_sVCDM, we find differences in the $\chi^2_{\min}$ values. Λ_sVCDM presents a lower $\chi^2_{\min}$ value for Planck-alone analysis and also when Planck data is combined with BAO/BAO($z > 0.8$) or PP&SH0ES data, but becomes indistinguishable when all the data are combined. This discrepancy is not surprising, as cosmological observables depend on the combined dynamics of the background and the perturbations, which can differ in GR and VCDM for the same background. In particular, the difference between Λ_sCDM and Λ_sVCDM in this cosmological context can be explained by two key points: (i) the mirror AdS-dS transition, and therefore the transition in the background evolution of the Universe, happens abruptly (instantaneously) in the Λ_sCDM model, whereas in the Λ_sVCDM model, the mirror AdS-dS transition is still fast but smoothly extended over a period of time, leading to a new brief temporary accelerated expansion era in the history of the universe; (ii) the VCDM gravity model distinctly provides the dynamics for the perturbations in the Λ_sVCDM model, including during the transition period, leading to extra terms in the cosmological perturbation equations. These terms are sensitive to the dynamics of the transition (both the background evolution and the dark energy, particularly, while it is undergoing the mirror AdS-dS transition) because they are influenced by the terms proportional to $\Lambda_{s,a}$, which is closely related to $\dot{H}$. In particular, we have managed to constrain the parameter $z_\dagger$ to $z_\dagger = 1.88^{+0.28}_{-0.58}$ at 68% CL even for the Planck-alone analysis of the Λ_sVCDM model, whereas for Λ_sCDM we have only a lower bound of $z_\dagger > 1.45$ at 95% CL. And, notably, the Planck-alone constraint obtained on H_0, viz., $H_0 = 73.4^{+1.8}_{-4.6}$ km s^{-1} Mpc^{-1}, turned out to be in excellent consistency with the latest SH0ES H_0 measurements [10,11,100], although we note that this improvement is still partly due to the degeneracy in the $z_\dagger$-H_0 plane, it is also significantly reflected in the mean H_0 value closely aligning with the SH0ES measurements. This result is nontrivial, as embedding Λ_sCDM into a gravity model could have deteriorated the success of the fit to the data, but in Λ_sVCDM, this does not happen, and some results are even more promising compared to the abrupt

---

[9] Thus, $\dot{H} \leq 0$ implies an upper limit on the rapidity of a smooth mirror AdS-dS transition within GR. A detailed investigation of this point is in progress and will be presented in an upcoming paper.

[10] By stability, we mean the absence of ghosts and/or gradient instabilities, allowing instead the standard Jeans instability for the pressureless components.

Λ_sCDM model. This demonstrates that the conjecture of Λ_sCDM can be successfully implemented into a predictive model, validating its consequences. More work is needed to further understand this improvement in the fit of Planck-alone data by Λ_sVCDM, not only by comparing it to Λ_sCDM but also to ΛCDM. In particular, we aim to understand the role played by the modified perturbation equations related to the transition and how the background transition itself may change the cosmological observables.

Finally, our findings in this work pave the way for another outcome: although different realizations of the Λ_sCDM framework within the VCDM gravity model, in line with the Λ_sVCDM model, seem to point in an interesting direction, there could be other implementations of Λ_sCDM, i.e., other theory embeddings, that might lead to even better fits to the data. We will pursue these research paths in future projects.

APPENDIX: THE VCDM MODEL

In this appendix, we briefly describe the VCDM model [39,40], a type II minimally modified gravity theory, in which the sign-switching cosmological constant (Λ_s) is embedded [38], setting the foundation for the model referred to as Λ_sVCDM in this paper. In the VCDM model, the usual cosmological constant (Λ) is replaced by a potential $V(\phi)$ of a nondynamical auxiliary field (ϕ), avoiding the introduction of extra physical degrees of freedom. The action for this theory is expressed as

$$S = S_m + M_P^2 \int d^4 x N \sqrt{\gamma} \left[\frac{1}{2} (R + K_{ij} K^{ij} - K^2) \right.$$
$$\left. - V(\phi) + \frac{\lambda_2}{N} \gamma^{ij} D_i D_j \phi - \frac{3\lambda^2}{4} - \lambda (K + \phi) \right], \quad \text{(A1)}$$

where S_m represents the sum of standard matter actions, N is the lapse function, and K_{ij} is the extrinsic curvature (with $K = \gamma^{ij} K_{ij}$ as its trace) relative to the 3D space metric γ_{ij} (which has an inverse γ^{ij}, determinant γ, and a covariant derivative D_i). The fields λ, λ_2, and ϕ are auxiliary fields. This modified gravity theory breaks four-dimensional diffeomorphism invariance but retains three-dimensional spatial diffeomorphism invariance and time-reparametrization invariance.

The VCDM theory is fully determined only after the potential $V(\phi)$ is specified, as the contribution of the auxiliary field ϕ to the Friedmann equation is given by $\rho_\phi \equiv M_P^2 (V - \phi V_{,\phi}) + \frac{3}{4} M_P^2 V_{,\phi}^2$, assuming a spatially flat Robertson-Walker metric, as in this work. Alternatively, one can specify the behavior of $\rho_\phi(\phi)$ and then determine the corresponding potential. In Eq. (2), we have specified the profile for $\Lambda_s(a) \equiv \rho_\phi(a)/M_P^2$, describing an effective smooth sign-switching cosmological constant within the VCDM framework, and then our modified Friedmann equation reads

$$3 M_P^2 H^2 = \rho(a) + M_P^2 \Lambda_s(a), \quad \text{(A2)}$$

where $\rho = \sum_I \rho_I$ is the total matter-energy density, with I running over all the matter components, including the dark matter. Each of these components satisfies the local energy-momentum conservation separately, meaning that each ρ_I is a known function of the scale factor a. This implies that $H(a)$ is fully determined. In VCDM, two other equations hold on a spatially flat RW background

$$a \frac{d\phi}{da} = \frac{3}{2} \frac{\rho + P}{M_P^2 H}, \quad \text{(A3)}$$

$$V = \frac{1}{3}\phi^2 - \frac{\rho}{M_P^2}, \qquad (A4)$$

where $P = \sum_I P_I$ is the total pressure for all standard matter components. Since $H = H(a)$ is now a known function of a, we can solve Eq. (A3) to find $\phi = \phi(a)$

after fixing the initial condition $\phi(a=1) = -3H_0$ (see [38]). Then, using Eq. (A4), we obtain the potential $V(\phi)$ (expressed in a parametric form). This process fully determines the Λ_sVCDM theory under consideration in this work. Finally, the modified equation for the perturbations, which can be directly deduced from the Lagrangian, was already given in Footnote 3.

[1] N. Aghanim *et al.* (Planck Collaboration), Planck 2018 results. VI. Cosmological parameters, Astron. Astrophys. **641,** A6 (2020); **652,** C4(E) (2021).

[2] S. Alam *et al.* (eBOSS Collaboration), Completed SDSS-IV extended Baryon Oscillation Spectroscopic Survey: Cosmological implications from two decades of spectroscopic surveys at the Apache Point Observatory, Phys. Rev. D **103,** 083533 (2021).

[3] S. Aiola *et al.* (ACT Collaboration), The Atacama Cosmology Telescope: DR4 maps and cosmological parameters, J. Cosmol. Astropart. Phys. 12 (2020) 047.

[4] M. Asgari *et al.* (KiDS Collaboration), KiDS-1000 cosmology: Cosmic shear constraints and comparison between two point statistics, Astron. Astrophys. **645,** A104 (2021).

[5] L. Balkenhol *et al.* (SPT-3G Collaboration), Measurement of the CMB temperature power spectrum and constraints on cosmology from the SPT-3G 2018 TT, TE, and EE dataset, Phys. Rev. D **108,** 023510 (2023).

[6] T. M. C. Abbott *et al.* (DES Collaboration), The Dark Energy Survey: Cosmology results with ∼1500 new high-redshift type Ia supernovae using the full 5-year dataset, arXiv:2401.02929.

[7] A. G. Adame *et al.* (DESI Collaboration), DESI 2024 VI: Cosmological constraints from the measurements of baryon acoustic oscillations, arXiv:2404.03002.

[8] L. Verde, T. Treu, and A. G. Riess, Tensions between the early and the late Universe, Nat. Astron. **3,** 891 (2019).

[9] E. Di Valentino *et al.*, Snowmass2021—Letter of interest cosmology intertwined II: The Hubble constant tension, Astropart. Phys. **131,** 102605 (2021).

[10] A. G. Riess *et al.*, A comprehensive measurement of the local value of the Hubble constant with 1 km/s/Mpc uncertainty from the Hubble Space Telescope and the SH0ES team, Astrophys. J. Lett. **934,** L7 (2022).

[11] L. Breuval, A. G. Riess, S. Casertano, W. Yuan, L. M. Macri, M. Romaniello, Y. S. Murakami, D. Scolnic, G. S. Anand, and I. Soszyński, Small magellanic cloud cepheids observed with the Hubble Space Telescope provide a new anchor for the SH0ES distance ladder, Astrophys. J. **973,** 30 (2024).

[12] Y. S. Murakami, A. G. Riess, B. E. Stahl, W. D. Kenworthy, D.-M. A. Pluck, A. Macoretta, D. Brout, D. O. Jones, D. M. Scolnic, and A. V. Filippenko, Leveraging SN Ia spectroscopic similarity to improve the measurement of H_0, J. Cosmol. Astropart. Phys. 11 (2023) 046.

[13] E. Di Valentino *et al.*, Cosmology intertwined III: $f\sigma_8$ and S_8, Astropart. Phys. **131,** 102604 (2021).

[14] S.-F. Chen, Z. Vlah, and M. White, A new analysis of galaxy 2-point functions in the BOSS survey, including full-shape information and post-reconstruction BAO, J. Cosmol. Astropart. Phys. 02 (2022) 008.

[15] P. A. Burger *et al.*, KiDS-1000 cosmology: Combined second- and third-order shear statistics, Astron. Astrophys. **683,** A103 (2024).

[16] A. Amon and G. Efstathiou, A non-linear solution to the S_8 tension?, Mon. Not. R. Astron. Soc. **516,** 5355 (2022).

[17] R. Dalal *et al.*, Hyper Suprime-Cam Year 3 results: Cosmology from cosmic shear power spectra, Phys. Rev. D **108,** 123519 (2023).

[18] T. M. C. Abbott *et al.* (Kilo-Degree Survey and Dark Energy Survey Collaborations), DES Y3 + KiDS-1000: Consistent cosmology combining cosmic shear surveys, Open J. Astrophys. **6** (2023), 10.21105/astro.2305.17173.

[19] S.-S. Li *et al.*, KiDS-1000: Cosmology with improved cosmic shear measurements, Astron. Astrophys. **679,** A133 (2023).

[20] J. Harnois-Deraps *et al.*, KiDS-1000 and DES-Y1 combined: Cosmology from peak count statistics, arXiv:2405.10312.

[21] E. Di Valentino, O. Mena, S. Pan, L. Visinelli, W. Yang, A. Melchiorri, D. F. Mota, A. G. Riess, and J. Silk, In the realm of the Hubble tension—A review of solutions, Classical Quantum Gravity **38,** 153001 (2021).

[22] E. Abdalla *et al.*, Cosmology intertwined: A review of the particle physics, astrophysics, and cosmology associated with the cosmological tensions and anomalies, J. High Energy Astrophys. **34,** 49 (2022).

[23] L. Perivolaropoulos and F. Skara, Challenges for ΛCDM: An update, New Astron. Rev. **95,** 101659 (2022).

[24] E. Di Valentino, Challenges of the standard cosmological model, Universe **8,** 399 (2022).

[25] M. Kamionkowski and A. G. Riess, The Hubble tension and early dark energy, Annu. Rev. Nucl. Part. Sci. **73,** 153 (2023).

[26] S. Vagnozzi, Seven hints that early-time new physics alone is not sufficient to solve the Hubble tension, Universe **9,** 393 (2023).

[27] O. Akarsu, E. O. Colgáin, A. A. Sen, and M. M. Sheikh-Jabbari, ΛCDM tensions: Localising missing physics through consistency checks, Universe **10,** 305 (2024).

[28] A. R. Khalife, M. B. Zanjani, S. Galli, S. Günther, J. Lesgourgues, and K. Benabed, Review of Hubble tension solutions with new SH0ES and SPT-3G data, J. Cosmol. Astropart. Phys. 04 (2024) 059.

[29] O. Akarsu, J. D. Barrow, L. A. Escamilla, and J. A. Vazquez, Graduated dark energy: Observational hints of a spontaneous sign switch in the cosmological constant, Phys. Rev. D **101**, 063528 (2020).

[30] O. Akarsu, S. Kumar, E. Özülker, and J. A. Vazquez, Relaxing cosmological tensions with a sign switching cosmological constant, Phys. Rev. D **104**, 123512 (2021).

[31] O. Akarsu, S. Kumar, E. Özülker, J. A. Vazquez, and A. Yadav, Relaxing cosmological tensions with a sign switching cosmological constant: Improved results with Planck, BAO, and Pantheon data, Phys. Rev. D **108**, 023513 (2023).

[32] O. Akarsu, E. Di Valentino, S. Kumar, R. C. Nunes, J. A. Vazquez, and A. Yadav, Λ_sCDM model: A promising scenario for alleviation of cosmological tensions, arXiv: 2307.10899.

[33] A. Yadav, S. Kumar, C. Kibris, and O. Akarsu, Λ_sCDM cosmology: Alleviating major cosmological tensions by predicting standard neutrino properties, arXiv:2406.18496.

[34] L. A. Anchordoqui, I. Antoniadis, and D. Lust, Anti-de Sitter $\to$ de Sitter transition driven by Casimir forces and mitigating tensions in cosmological parameters, Phys. Lett. B **855**, 138775 (2024).

[35] L. A. Anchordoqui, I. Antoniadis, D. Lust, N. T. Noble, and J. F. Soriano, From infinite to infinitesimal: Using the Universe as a dataset to probe Casimir corrections to the vacuum energy from fields inhabiting the dark dimension, arXiv:2404.17334.

[36] I. Antoniadis, L. A. Anchordoqui, and D. Lust, Landscape, swampland and extra dimensions, Proc. Sci. CORFU2023 (**2024**) 215 [arXiv:2405.04427].

[37] B. Alexandre, S. Gielen, and J. Magueijo, Overall signature of the metric and the cosmological constant, J. Cosmol. Astropart. Phys. 02 (2024) 036.

[38] O. Akarsu, A. De Felice, E. Di Valentino, S. Kumar, R. C. Nunes, E. Ozulker, J. A. Vazquez, and A. Yadav, Λ_sCDM cosmology from a type-II minimally modified gravity, arXiv:2402.07716.

[39] A. De Felice, A. Doll, and S. Mukohyama, A theory of type-II minimally modified gravity, J. Cosmol. Astropart. Phys. 09 (2020) 034.

[40] A. De Felice, S. Mukohyama, and M. C. Pookkillath, Addressing H_0 tension by means of VCDM, Phys. Lett. B **816**, 136201 (2021); **818**, 136364(E) (2021).

[41] A. De Felice, A. Doll, F. Larrouturou, and S. Mukohyama, Black holes in a type-II minimally modified gravity, J. Cosmol. Astropart. Phys. 03 (2021) 004.

[42] A. De Felice and S. Mukohyama, Weakening gravity for dark matter in a type-II minimally modified gravity, J. Cosmol. Astropart. Phys. 04 (2021) 018.

[43] A. De Felice, S. Mukohyama, and M. C. Pookkillath, Static, spherically symmetric objects in type-II minimally modified gravity, Phys. Rev. D **105**, 104013 (2022).

[44] A. De Felice, K.-i. Maeda, S. Mukohyama, and M. C. Pookkillath, Comparison of two theories of type-IIa minimally modified gravity, Phys. Rev. D **106**, 024028 (2022).

[45] K. Dutta, Ruchika, A. Roy, A. A. Sen, and M. M. Sheikh-Jabbari, Beyond ΛCDM with low and high redshift data: Implications for dark energy, Gen. Relativ. Gravit. **52**, 15 (2020).

[46] L. Visinelli, S. Vagnozzi, and U. Danielsson, Revisiting a negative cosmological constant from low-redshift data, Symmetry **11**, 1035 (2019).

[47] A. Perez, D. Sudarsky, and E. Wilson-Ewing, Resolving the H_0 tension with diffusion, Gen. Relativ. Gravit. **53**, 7 (2021).

[48] E. Di Valentino, A. Mukherjee, and A. A. Sen, Dark energy with phantom crossing and the H_0 tension, Entropy **23**, 404 (2021).

[49] G. Acquaviva, O. Akarsu, N. Katirci, and J. A. Vazquez, Simple-graduated dark energy and spatial curvature, Phys. Rev. D **104**, 023505 (2021).

[50] A. A. Sen, S. A. Adil, and S. Sen, Do cosmological observations allow a negative Λ?, Mon. Not. R. Astron. Soc. **518**, 1098 (2022).

[51] E. Ozulker, Is the dark energy equation of state parameter singular?, Phys. Rev. D **106**, 063509 (2022).

[52] S. Di Gennaro and Y. C. Ong, Sign switching dark energy from a running barrow entropy, Universe **8**, 541 (2022).

[53] H. Moshafi, H. Firouzjahi, and A. Talebian, Multiple transitions in vacuum dark energy and H_0 tension, Astrophys. J. **940**, 121 (2022).

[54] A. van de Venn, D. Vasak, J. Kirsch, and J. Struckmeier, Torsional dark energy in quadratic gauge gravity, Eur. Phys. J. C **83**, 288 (2023).

[55] Y. C. Ong, An effective sign switching dark energy: Lotka–Volterra model of two interacting fluids, Universe **9**, 437 (2023).

[56] Y. Tiwari, B. Ghosh, and R. K. Jain, Towards a possible solution to the Hubble tension with Horndeski gravity, Eur. Phys. J. C **84**, 220 (2024).

[57] J. A. Vázquez, D. Tamayo, G. Garcia-Arroyo, I. Gómez-Vargas, I. Quiros, and A. A. Sen, Coupled multiscalar field dark energy, Phys. Rev. D **109**, 023511 (2024).

[58] S. A. Adil, O. Akarsu, E. Di Valentino, R. C. Nunes, E. Özülker, A. A. Sen, and E. Specogna, Omnipotent dark energy: A phenomenological answer to the Hubble tension, Phys. Rev. D **109**, 023527 (2024).

[59] S. A. Adil, U. Mukhopadhyay, A. A. Sen, and S. Vagnozzi, Dark energy in light of the early JWST observations: Case for a negative cosmological constant?, J. Cosmol. Astropart. Phys. 10 (2023) 072.

[60] E. A. Paraskevas and L. Perivolaropoulos, The density of virialized clusters as a probe of dark energy, Mon. Not. R. Astron. Soc. **531**, 1021 (2024).

[61] R. Y. Wen, L. T. Hergt, N. Afshordi, and D. Scott, A cosmic glitch in gravity, J. Cosmol. Astropart. Phys. 03 (2024) 045.

[62] N. Menci, S. A. Adil, U. Mukhopadhyay, A. A. Sen, and S. Vagnozzi, Negative cosmological constant in the dark energy sector: Tests from JWST photometric and spectroscopic observations of high-redshift galaxies, arXiv:2401 .12659.

[63] A. Gomez-Valent and J. Sola Peracaula, Phantom matter: A challenging solution to the cosmological tensions, arXiv:2404.18845.

[64] A. D. Felice, S. Kumar, S. Mukohyama, and R. C. Nunes, Observational bounds on extended minimal theories of massive gravity: New limits on the graviton mass, J. Cosmol. Astropart. Phys. 04 (2024) 013.

[65] M. T. Manoharan, Insights on Granda–Oliveros holographic dark energy: Possibility of negative dark energy at $z \gtrsim 2$, Eur. Phys. J. C **84**, 552 (2024).

[66] V. Sahni, A. Shafieloo, and A. A. Starobinsky, Model independent evidence for dark energy evolution from baryon acoustic oscillations, Astrophys. J. Lett. **793**, L40 (2014).

[67] E. Aubourg *et al.* (BOSS Collaboration), Cosmological implications of baryon acoustic oscillation measurements, Phys. Rev. D **92**, 123516 (2015).

[68] V. Poulin, K. K. Boddy, S. Bird, and M. Kamionkowski, Implications of an extended dark energy cosmology with massive neutrinos for cosmological tensions, Phys. Rev. D **97**, 123504 (2018).

[69] Y. Wang, L. Pogosian, G.-B. Zhao, and A. Zucca, Evolution of dark energy reconstructed from the latest observations, Astrophys. J. Lett. **869**, L8 (2018).

[70] R. Calderón, R. Gannouji, B. L'Huillier, and D. Polarski, Negative cosmological constant in the dark sector?, Phys. Rev. D **103**, 023526 (2021).

[71] A. Bonilla, S. Kumar, and R. C. Nunes, Measurements of H_0 and reconstruction of the dark energy properties from a model-independent joint analysis, Eur. Phys. J. C **81**, 127 (2021).

[72] L. A. Escamilla and J. A. Vazquez, Model selection applied to reconstructions of the dark energy, Eur. Phys. J. C **83**, 251 (2023).

[73] R. C. Bernardo, D. Grandón, J. Said Levi, and V. H. Cárdenas, Parametric and nonparametric methods hint dark energy evolution, Phys. Dark Universe **36**, 101017 (2022).

[74] O. Akarsu, E. O. Colgain, E. Özulker, S. Thakur, and L. Yin, Inevitable manifestation of wiggles in the expansion of the late Universe, Phys. Rev. D **107**, 123526 (2023).

[75] R. C. Bernardo, D. Grandón, J. Levi Said, and V. H. Cárdenas, Dark energy by natural evolution: Constraining dark energy using approximate Bayesian computation, Phys. Dark Universe **40**, 101213 (2023).

[76] M. Malekjani, R. M. Conville, E. O. Colgáin, S. Pourojaghi, and M. M. Sheikh-Jabbari, On redshift evolution and negative dark energy density in Pantheon+ Supernovae, Eur. Phys. J. C **84**, 317 (2024).

[77] L. A. Escamilla, O. Akarsu, E. Di Valentino, and J. A. Vazquez, Model-independent reconstruction of the interacting dark energy kernel: Binned and Gaussian process, J. Cosmol. Astropart. Phys. 11 (2023) 051.

[78] A. Gómez-Valent, A. Favale, M. Migliaccio, and A. A. Sen, Late-time phenomenology required to solve the H0 tension in view of the cosmic ladders and the anisotropic and angular BAO datasets, Phys. Rev. D **109**, 023525 (2024).

[79] R. Medel-Esquivel, I. Gómez-Vargas, A. A. M. Sánchez, R. García-Salcedo, and J. Alberto Vázquez, Cosmological parameter estimation with genetic algorithms, Universe **10**, 11 (2024).

[80] R. Calderon *et al.* (DESI Collaboration), DESI 2024: Reconstructing dark energy using crossing statistics with DESI DR1 BAO data, arXiv:2405.04216.

[81] D. Bousis and L. Perivolaropoulos, Hubble tension tomography: BAO vs SnIa distance tension, arXiv:2405.07039.

[82] H. Wang, Z.-Y. Peng, and Y.-S. Piao, Can recent DESI BAO measurements accommodate a negative cosmological constant?, arXiv:2406.03395.

[83] E. O. Colgáin, S. Pourojaghi, and M. M. Sheikh-Jabbari, Implications of DES 5YR SNe dataset for ΛCDM, arXiv:2406.06389.

[84] M. A. Sabogal, O. Akarsu, A. Bonilla, E. Di Valentino, and R. C. Nunes, Exploring new physics in the late Universe's expansion through non-parametric inference, Eur. Phys. J. C **84**, 703 (2024).

[85] D. Blas, J. Lesgourgues, and T. Tram, The cosmic linear anisotropy solving system (CLASS). Part II: Approximation schemes, J. Cosmol. Astropart. Phys. 07 (2011) 034.

[86] B. Audren, J. Lesgourgues, K. Benabed, and S. Prunet, Conservative constraints on early cosmology with monte python, J. Cosmol. Astropart. Phys. 02 (2013) 001.

[87] T. Brinckmann and J. Lesgourgues, MontePython 3: Boosted MCMC sampler and other features, Phys. Dark Universe **24**, 100260 (2019).

[88] A. Gelman and D. B. Rubin, Inference from iterative simulation using multiple sequences, Stat. Sci. **7**, 457 (1992).

[89] N. Aghanim *et al.* (Planck Collaboration), Planck 2018 results. V. CMB power spectra and likelihoods, Astron. Astrophys. **641**, A5 (2020).

[90] N. Aghanim *et al.* (Planck Collaboration), Planck 2018 results. VIII. Gravitational lensing, Astron. Astrophys. **641**, A8 (2020).

[91] J.-P. Uzan and C. Pitrou, The Hubble tension as a window on the gravitation of the dark matter sector: Exploration of a family of models, Phys. Rev. D **109**, 103505 (2024).

[92] C. Pitrou and J.-P. Uzan, The Hubble tension as a window on the gravitation of the dark matter sector, Phys. Rev. Lett. **132**, 191001 (2024).

[93] T. M. C. Abbott *et al.* (DES Collaboration), Dark Energy Survey: A 2.1% measurement of the angular Baryonic Acoustic Oscillation scale at redshift $z_{\mathrm{eff}} = 0.85$ from the final dataset, Phys. Rev. D **110**, 063515 (2024).

[94] D. Scolnic *et al.*, The Pantheon + analysis: The full data set and light-curve release, Astrophys. J. **938**, 113 (2022).

[95] K. Kuijken *et al.*, The fourth data release of the Kilo-Degree Survey: Ugri imaging and nine-band optical-IR photometry over 1000 square degrees, Astron. Astrophys. **625**, A2 (2019).

[96] B. Giblin *et al.*, KiDS-1000 catalogue: Weak gravitational lensing shear measurements, Astron. Astrophys. **645**, A105 (2021).

[97] H. Hildebrandt *et al.*, KiDS-1000 catalogue: Redshift distributions and their calibration, Astron. Astrophys. **647**, A124 (2021).

[98] A. Mead, J. Peacock, C. Heymans, S. Joudaki, and A. Heavens, An accurate halo model for fitting non-linear cosmological power spectra and baryonic feedback models, Mon. Not. R. Astron. Soc. **454**, 1958 (2015).

[99] D. Valcin, R. Jimenez, L. Verde, J. L. Bernal, and B. D. Wandelt, The age of the Universe with globular clusters: Reducing systematic uncertainties, J. Cosmol. Astropart. Phys. 08 (2021) 017.

[100] S. A. Uddin *et al.*, Carnegie Supernova Project-I and -II: Measurements of H_0 using cepheid, TRGB, and SBF distance calibration to type Ia supernovae, Astrophys. J. **970**, 72 (2024).

[101] A. G. Adame *et al.* (DESI Collaboration), DESI 2024 III: Baryon Acoustic Oscillations from galaxies and quasars, arXiv:2404.03000.

[102] A. G. Adame *et al.* (DESI Collaboration), DESI 2024 IV: Baryon acoustic oscillations from the Lyman alpha forest, arXiv:2404.03001.

[103] W. Giarè, M. A. Sabogal, R. C. Nunes, and E. Di Valentino, Interacting dark energy after DESI baryon acoustic oscillation measurements, arXiv:2404.15232.

[104] P. Mukherjee and A. A. Sen, Model-independent cosmological inference post DESI DR1 BAO measurements, arXiv:2405.19178.

[105] G. Ye, M. Martinelli, B. Hu, and A. Silvestri, Non-minimally coupled gravity as a physically viable fit to DESI 2024 BAO, arXiv:2407.15832.

[106] W. Giarè, M. Najafi, S. Pan, E. Di Valentino, and J. T. Firouzjaee, Robust preference for dynamical dark energy in DESI BAO and SN measurements, arXiv:2407.16689.

[107] B. R. Dinda and R. Maartens, Model-agnostic assessment of dark energy after DESI DR1 BAO, arXiv:2407.17252.

[108] J.-Q. Jiang, D. Pedrotti, S. S. da Costa, and S. Vagnozzi, Non-parametric late-time expansion history reconstruction and implications for the Hubble tension in light of DESI, arXiv:2408.02365.

[109] S. Vagnozzi, F. Pacucci, and A. Loeb, Implications for the Hubble tension from the ages of the oldest astrophysical objects, J. High Energy Astrophys. **36**, 27 (2022).

[110] V. Poulin, T. L. Smith, and T. Karwal, The ups and downs of early dark energy solutions to the Hubble tension: A review of models, hints and constraints circa 2023, Phys. Dark Universe **42**, 101348 (2023).

[111] J. L. Bernal, L. Verde, R. Jimenez, M. Kamionkowski, D. Valcin, and B. D. Wandelt, The trouble beyond H_0 and the new cosmic triangles, Phys. Rev. D **103**, 103533 (2021).

[112] M. Boylan-Kolchin and D. R. Weisz, Uncertain times: The redshift–time relation from cosmology and stars, Mon. Not. R. Astron. Soc. **505**, 2764 (2021).

[113] A. R. Liddle, Information criteria for astrophysical model selection, Mon. Not. R. Astron. Soc. **377**, L74 (2007).

[114] A. Heavens, Y. Fantaye, E. Sellentin, H. Eggers, Z. Hosenie, S. Kroon, and A. Mootovaloo, No evidence for extensions to the standard cosmological model, Phys. Rev. Lett. **119**, 101301 (2017).

[115] A. Heavens, Y. Fantaye, A. Mootoovaloo, H. Eggers, Z. Hosenie, S. Kroon, and E. Sellentin, Marginal likelihoods from Monte Carlo Markov chains, arXiv:1704.03472.

[116] R. E. Kass and A. E. Raftery, Bayes factors, J. Am. Stat. Assoc. **90**, 773 (1995).

[117] R. Trotta, Bayes in the sky: Bayesian inference and model selection in cosmology, Contemp. Phys. **49**, 71 (2008).

[118] W. Handley, FGIVENX: A Python package for functional posterior plotting, J. Open Source Software **3**, 849 (2018).

[119] J. D. Barrow, Sudden future singularities, Classical Quantum Gravity **21**, L79 (2004).

[120] E. A. Paraskevas, A. Cam, L. Perivolaropoulos, and O. Akarsu, Transition dynamics in the ΛsCDM model: Implications for bound cosmic structures, Phys. Rev. D **109**, 103522 (2024).